Simulation Study of Shape Memory Alloys for Elastocaloric Application

M-Tech Thesis

By

TIWARI SATYAM SURENDRA

DEPARTMENT OF MECHANICAL ENGINEERING

INDIAN INSTITUTE OF TECHNOLOGY INDORE

MAY 2025

Simulation Study of Shape Memory Alloys for Elastocaloric Application

A THESIS

Submitted in partial fulfillment of the

requirements for the award of the degree

of

Master of Technology

by

TIWARI SATYAM SURENDRA

DEPARTMENT OF MECHANICAL ENGINEERING

INDIAN INSTITUTE OF TECHNOLOGY INDORE

MAY 2025

INDIAN INSTITUTE OF TECHNOLOGY INDORE

CANDIDATE'S DECLARATION

I hereby certify that the work which is being presented in the thesis entitled **Simulation Study of Shape Memory Alloys for Elastocaloric Application** in the partial fulfillment of the requirements for the award of the degree of **MASTER OF TECHNOLOGY** and submitted in the **DEPARTMENT OF MECHANICAL ENGINEERING, Indian Institute of Technology Indore,** is an authentic record of my own work carried out during the time period from June 2024 to May 2025 under the supervision of Dr. Satyanarayan Patel, Associate Professor, Department of Mechanical Engineering, IIT Indore.

The matter in this thesis has not been submitted by me for the award of any other degree of this or any other institute.

05/Jun/2025

Signature of the student with the date
(TIWARI SATYAM SURENDRA)

This is to certify that the above statement made by the candidate is correct to the best of my/our knowledge.

05/06/2025

Signature of the Supervisor of
M-Tech thesis (with date)
(Dr. Satyanarayan Patel)

TIWARI SATYAM SURENDRA has successfully given his M-Tech Oral Examination held on **26th May 2025**.

Signature(s) of Supervisor(s) of M-Tech thesis

Date: 05/06/2025

Convener, DPGC

Date: 05-06-2025

ACKNOWLEDGEMENTS

I sincerely thank my supervisor **Dr. Satyanarayan Patel** for invigorating motivation and guidance. He constantly supported the necessary facilities to complete the work within the stipulated tenure. His consistent discussions have yielded fruitful suggestions and ideas for comprehensively completing the thesis work. He has taught me the value of hard work in any profession and ethics, which helped me swiftly through the rollercoaster of M-Tech.

I thank **Prof. Suhas Joshi,** Director, IIT Indore, and **Prof. Shanmugan Dhinakaran**, Head, Department of Mechanical Engineering, for providing this opportunity and support to conduct my research. I'm grateful to the program coordinator, **Dr. Harekrishna Yadav**, for organizing the M-Tech schedule and the thermal faculty members' valuable suggestions.

I sincerely thank Senior **Dr. Nishchay Saurabh**, **Mr. Aditya Gaur, Mr. Mohit Singhal, and Mr. Dhiraj Singh** for their constant support, mentorship, and direction throughout M-Tech project. I also want to thank all my friends for their encouragement and support, without which this journey is incomplete.

Finally, I would like to thank my family for their love, support, and constant trust throughout life, which has enabled me to be the better person I am today.

I thank the Indian Science Technology and Engineering facilities Map (I-STEM), a program supported by the office of the Principal Scientific Adviser to the Govt of India, for enabling access to the COMSOL Multiphysics software suite used to carry out this work.

Dedicated to

महादेव

ABSTRACT

In recent years, the need for alternative cooling technologies has been in high demand due to increased electronic temperature and miniaturization of electronics. The present study discusses elastocaloric (eC) as a viable device that can solve the challenges of small-scale cooling applications. In the elastocaloric, the cyclic stress loading/unloading is applied to change the temperature. The analysis proceeds systematically to examine relevant parameters. Initially, modeling is conducted using the COMSOL Multiphysics software to explore the impact of various factors. Equation-based help estimate the elastocaloric effect. In the initial part, the results available in the literature are validated using a trapezoidal stress field. The stress field is applied quickly while the holding time is varied to check for when the material comes to normal temperature after loading and unloading. As a built-in elastocaloric module is unavailable, the current study uses the heat transfer equation available in heat transfer modules. The modeling has been discussed in detail.

It is found that the stress magnitude, holding time, and operating temperature play a vital role in obtaining the maximum eC effect. Finally, an application is considered to cool a chip at an initial temperature of 313.15 K and generate a heat of 1 W, with dimensions of 15 mm x 15 mm x 2 mm. The results show that eC is more effective than traditional methods for cooling the same device. The study is insightful and paves the way for further exploration of the proposed eC devices for cooling automotive headlamps, inspiring future research and development in this field.

TABLE OF CONTENTS

Chapter 5: Conclusion and Future Outlook

LIST OF FIGURES

LIST OF TABLES

NOMENCLATURE

C_p	Heat Capacity at Constant Pressure
G	Gibbs Free Energy
k	Thermal Conductivity
m	Mass
Q	Heat Source
Q_{ted}	Heat Generated due to Thermoelastic Damping
S	Entropy
ΔS	Entropy Change
T	Temperature
ΔT	Temperature Change
ΔT_{ad}	Adiabatic Temperature Change
t	Time
t_h	Holding Time
U	Internal Energy
W	Work done by the outside
ε	Strain
ε	Transformation strain
ρ	Density of an elastocaloric material
σ	Stress

ACRONYMS

SMA	Shape Memory Alloy
COP	Coefficient of Performance
eC	Elastocaloric
ECE	Electrocaloric Effect
eCE	Elastocaloric Effect
HCFC	Hydrochlorofluorocarbons
MCE	Magnetocaloric Effect
MD	Molecular Dynamics
VC	Vapor Compression
HVAC	Heating Ventilation and Air Conditioning
CFC	Chlorofluorocarbons

Chapter 1

Introduction

1.1 Introduction & motivation

The world's 20% electricity consumption is used for refrigeration applications [1]. In this direction, vapor compression refrigeration is the most widely used technology. However, no specific technology exists for miniature-scale cooling applications. Vapor compression refrigeration and air conditioning dominate commercial buildings and residential applications because of their higher efficiency, safety, lower manufacturing and operation costs. However, it has an environmental impact due to the leakage of hazardous refrigerants, causing the greenhouse effect, which leads to the depletion of the ozone layer and is a major contributor to climate change. Thus, it has necessitated the search for alternative cooling technologies suitable for miniature and large-scale applications. The major cooling applications lie in storing, transporting, and producing foodstuffs, medical supplies, and healthcare. However, the challenges of available vapor compression technology necessitate a search for alternative cooling technologies utilized for micro-scale applications, which is a more complex field than macroscale applications. As per the Kigali amendment, the application of hydrofluorocarbons (HFCs) is also to be reduced due to their high global warming potential (~14000) [2]. In 2014, a report published by the U.S. Department of Energy about the energy-saving potential of non-vapor compression HVAC technologies claimed that elastocaloric/thermoelastic cooling could be the most potent replacement for heating and cooling applications. The advantage of elastocaloric (eC) cooling is that the material is solid, has almost zero global warming potential, is applied as a refrigerant, and has maximum heat transfer potential compared to other alternative cooling technologies.

Cooling has a remarkable effect on energy usage in refrigeration and air conditioning in the residential sector, transport of food items, medication, and industrial cooling. According to the Montreal Protocol, chlorofluorocarbons (CFCs) and hydrochlorofluorocarbons (HCFCs) are phased out because of their ozone-depleting properties. Modifications to refrigerants over time have led to reduced environmental impacts. Despite numerous technological advancements, it has still been proven to have adverse effects due to the large-scale adoption of the technology. Hence, there is a sincere need for new environmentally friendly technologies for microscale and large-scale residential cooling applications. In modern electronics, efficient heat management is essential. High temperatures can affect their reliability and lifespan as society increasingly depends on battery-powered devices like smartphones, tablets, computers, personal digital assistants, iPods, solar modules, and electric vehicles. It is found that approximately 55% of product failures are related to high-temperature operations [3]. Thus, a small-

scale cooling technology is needed for the electronics. In this direction, various cooling technologies are available. The classification of the cooling technology is given in section 1.2.

1.2 Classification of cooling technologies

As per the temperature classification section of Indian standards, the refrigerating appliances are classified into SN, N, ST and Tr as per temperature ranges where SN is subnormal/extended temperate, which is suitable in a temperature range of 10-32 ℃, N is normal, i.e., suitable in temperature range 16-32 ℃; ST is subtropical which is suitable in 16-38 ℃ and Tr is tropical which suits temperature range of 16-43 ℃ [4].

1.2.1 Classification based on primary energy input

Figure 1.1 shows various cooling technologies classified based on the method of trigger force applied,

A. Based on electrical input

1. Thermoelectric cooling operates based on the Peltier effect, which creates a temperature difference when an electric current flows through the junction of two dissimilar materials. The device's low efficiency (5-15%) poses a major challenge, along with limited power output, mechanical fatigue, material constraints, and high cost [5]. It remains the most common technology despite its limitations.

2. Thermionic cooling is a solid-state cooling technique based on the thermionic emission of electrons. In this process, high-energy (hot) electrons are emitted from a material (usually a low-work-function emitter) across a vacuum or semiconductor barrier to a collector at a lower temperature, effectively removing heat from the emitter side [6]. Due to lower efficiency at low temperatures, material challenges, fabrication difficulties, and high cost, its application is limited to microelectronics [7].

3. Electrocaloric cooling is discussed in section 1.3, along with Table 1.1. It is a technology under development and can be applied for electronic cooling, though with some limitations.

B. Based on mechanical input

1. Vapor compression is the most developed technology in current operation, although it has the disadvantage of hazardous refrigerants, which pollute the environment due to leakage and cause global warming. Its applications range from small purposes like households to large-scale cooling like malls and factories.

2. Many technologies in mechanical input show no phase change, which can be further classified as gas-based and solid-based materials. The solid-based material is called the elastomeric/thermoelastic/eC cooling method, which is discussed in detail in section 1.4.

Other non-phase change technologies without phase change are

a. The pulse tube uses oscillating helium gas in a regenerator and pulse tube. Heat is absorbed at the cold end (via expansion) and rejected at the hot end through heat exchangers. It applies to cryogenic cooling, like space sensors and ultra-low temperature systems. It has low efficiency, complex design, and low cooling power.
Suitable only in very low-temperature applications and higher costs [8].

b. The ejector operates on high-pressure primary gas that accelerates through a nozzle, entraining low-pressure secondary gas. Momentum transfer compresses the mixed flow. It finds application in cryogenics and low-grade heat recovery. However, lower coefficient of performance (COP) and design complications restrict its application [9].

c. In a vortex tube, compressed gas enters tangentially, creating a high-speed vortex. The outer (hot) stream exits one end, while the inner (cold) stream exits the opposite end. It is applied in spot cooling of tools and emergency cooling in hazardous environments. Still, its low COP, limited use in small-scale cooling, and noisy operation restrict its wider application [10].

d. Reverse Stirling cryocoolers mechanically drive gas through compression/expansion phases via pistons. Heat is pumped from the cold to the hot ends. It finds application in infrared (IR) detectors, cryogenic sensors, and helium liquefaction, but wear, vibrations, and cost limit its applications.

e. The reverse Ericsson cycle is similar to Stirling but uses isothermal compression/expansion, which requires near-ideal regeneration. Hence, it rarely finds application. Efficiency is constrained by regenerator heat conductance [11].

f. In a reverse Brayton cryocooler, gas is compressed, precooled, expanded in a turbine, and then absorbs heat. It operates with turbomachinery (no pistons). It finds applications in large-scale cryogenics and satellite thermal management. High-cost turbomachinery and low small-scale efficiency limit its application [12].

C. Based on acoustic input

Thermoacoustic cooling transfers heat through high-amplitude sound waves, relying on no refrigerants or moving parts except the driver. It finds application in domestic cooling, space technology, cryogenics, etc. Despite this, low efficiency, noise, and scalability remain challenges [13].

D. Based on magnetic input

Magnetocaloric cooling employs a magnetic field as a solid-state cooling technology based on caloric effects, discussed in section 1.3 and Table 1.1.

E. Based on chemical input

a. Desiccant cooling is a three-step process, i.e., dehumidification, cooling, and regeneration. First, the humid air passes through a desiccant (silica gel/lithium chloride), which absorbs moisture; then, the dried air is cooled sensibly using heat exchangers, and finally, the desiccant is heated to restore drying capacity.

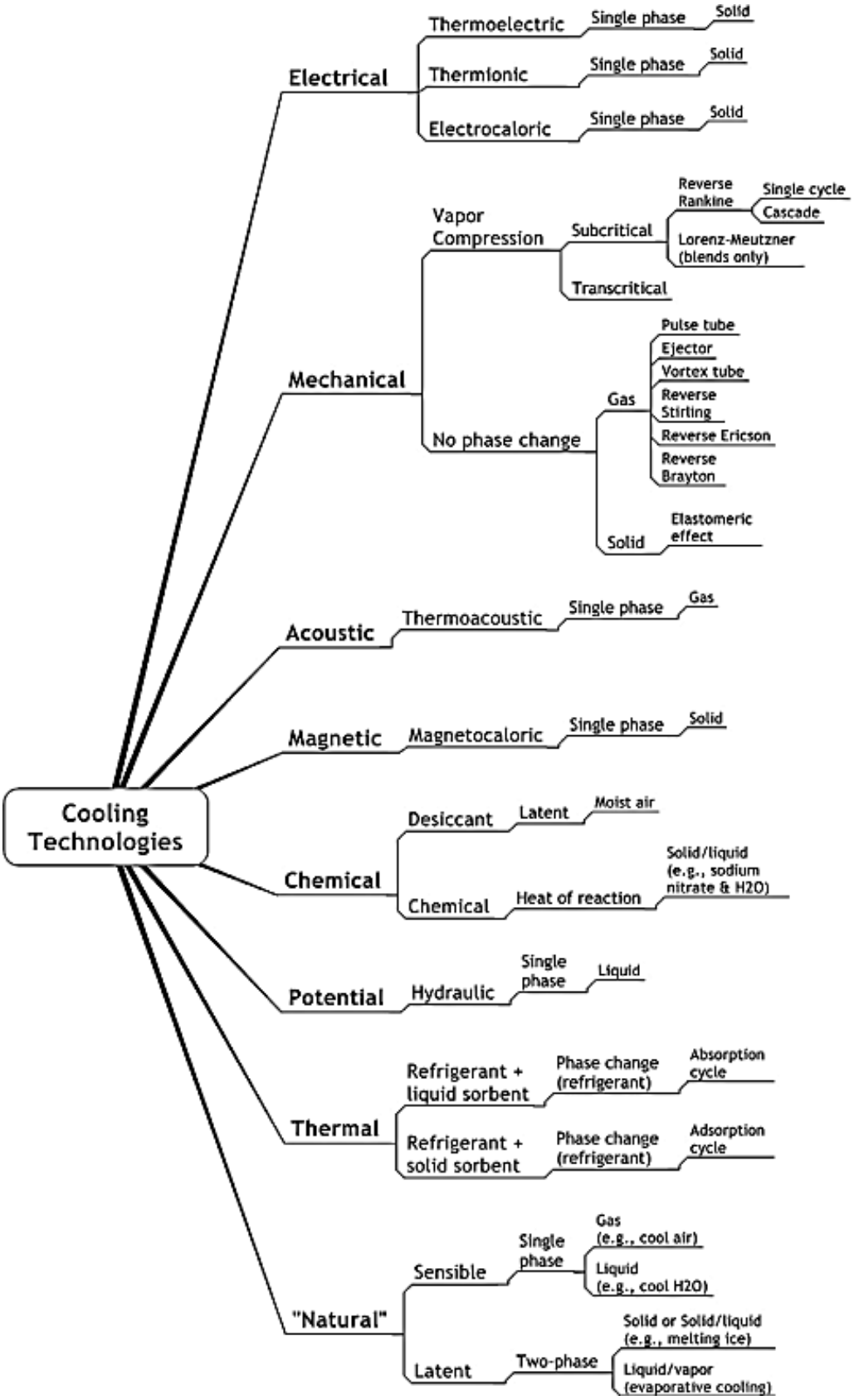

Fig. 1.1. classification of cooling technologies [14].

It finds applications in healthcare, food processing, etc. Despite these benefits, the high initial cost, corrosion risks, and maintenance limit its applications in India [15].

b. Chemical cooling, based on the heat of reaction, relies on endothermic reactions to absorb heat from surroundings, achieving cooling; for example, when NH_4NO_3 is dissolved in water, it absorbs heat and causes cooling. It finds application in instant cold packs, cryogenic gas separation, etc. Nevertheless, it is not always practical due to material constraints and precise stoichiometry for cooling [16].

F. Based on potential as input

Hydraulic refrigeration relies on hydraulic compression with a liquid, such as water, instead of mechanical compression to pressurize the refrigerant in a vertical column. Its applications include medium-scale cooling in chemical plants, food processing, and waste heat utilization. Still, its complex design, low efficiency, and maintenance requirements make it less preferable [17].

G. Based on thermal input

a. Refrigerant with liquid sorbent (absorption cooling) considers heat to separate refrigerant (e.g., ammonia) from a liquid sorbent, then condenses and expands it to absorb heat. Applications include solar cooling and industrial refrigeration but suffer from low efficiency, slow response, and complexity [18].

b. Refrigerants with solid sorbents apply solid sorbents (e.g., silica gel, zeolites, or complex compounds) to adsorb refrigerant vapors (e.g., ammonia, water, or hydrocarbons), enabling heat-driven refrigeration. Its applications are in solar cooling and waste heat recovery, although it is bulky and has a very low COP [19].

H. Based on a natural phenomenon

a. Sensible cooling takes ambient air/water for heat removal without moisture condensation; its applications are building cooling at night in summer. However, it may be less valuable in high humidity [20].

b. Latent cooling uses evaporation or phase-change materials (PCMs) to absorb heat; its application is passive cooling. Moreover, it faces challenges in a humid environment [21].

1.2.2 Classification of solid-state cooling technologies

The solid-state cooling technologies, which are discussed in Chapter 1.3, are classified based on the field required to trigger the effect as magnetocaloric, electrocaloric, barocaloric, and eC to the applied field, magnetic, electric, hydrostatic pressure, and unidirectional stress, respectively [22]. In Table 1.1, the principle of working, Carnot COP, environmental impact, and current status of the solid-state technologies have been tabulated compared to vapor compression refrigeration and thermoelectric cooling methods, which are applied extensively despite environmental and performance challenges.

1.3 Solid state cooling

Solid-state cooling technology is based on caloric effects in solid materials, which act as refrigerants under cyclic loads. A caloric effect is a reversible thermal

change in a material induced by an external magnetic, electric, or mechanical field. Applying the specific driving field in such caloric materials triggers the isothermal change in entropy or adiabatic temperature [23, 24]. Based on the external field applied to materials, the cooling method is named magnetocaloric, electrocaloric, barocaloric, and eC, where the respective field applied is magnetic, electric, hydrostatic pressure, and unidirectional stress [22]. Compressors and liquid and vapor refrigerants can be eliminated using solid-state materials [22]. Among the different caloric cooling technologies, the cooling based on magnetic effect, i.e., magnetocaloric, is the most researched, as reported in Figure 1.2. The magnetocaloric effect requires a large magnetic field for entropy change, and the materials involved are rare-earth or transitional metals like gadolinium (Gd), lanthanum (La), rhodium (Rh), etc., which are expensive [25].

Table 1.1. Comparison between VCR and solid-state cooling technologies [26].

Technology	**Principle**	**COP / COP_{carnot}**	**Environmental impact**	**Current state**
Vapor compression refrigeration	Vaporization latent heat	~60%	High	Commercial
Thermoelectric	Peltier effect	~10%	Low	Commercial
Magnetocaloric	Magnetic field induced	~70%	Low	Prototype
Electrocaloric	Polarization-induced entropy change	~60%	Low	Prototype
Barocaloric	Volumetric strain-induced entropy change	-	Low	Prototype
Elastocaloric	Strain-induced entropy change	~83%	Low	Prototype

Also, research in electrocaloric has followed magnetocaloric. It has been found that electrocaloric materials fail due to electrical breakdown under a high field. Improvement in contact with electrodes, decreased thickness, and chemical composition are other factors that improve cooling [25]. The materials for electrocaloric can be lead-based ceramics like lead zirconium titanate (PZT), lead scandium titanate (PST), and lead scandium niobate (PSN), which are hazardous; hence lead lead-free ceramic perovskite oxides like barium titanate (BTO), sodium-bismuth titanate (NBT) are also considered [27]. Electrocaloric polymer polyvinylidene fluoride is applied for the relaxor ferroelectric property [28]. Barocaloric cooling is based on isostatic pressure, which induces a volume change that results in a change in entropy [29]. Although this effect is present in

all materials, challenges in applying pressure and experimentally measuring the barocaloric effect remain [30]. EC cooling is an emerging field in caloric cooling due to an externally applied uniaxial stress field [31, 32], discussed in detail in section 1.4.

Figure 1.2 shows how research in solid-state cooling technologies is emerging. The plot is based on reported prototypes developed over the years mentioned. It is clear that the research and prototype development in the field of magnetocaloric started first, dating back to 1975; electrocaloric was the second technology, and the prototype was developed in the 19th century [32]. However, the amount of research in magnetocaloric has not yet yielded a model that significantly affects cooling and refrigeration applications. Comparatively, eC is a newer technology, about a decade old.

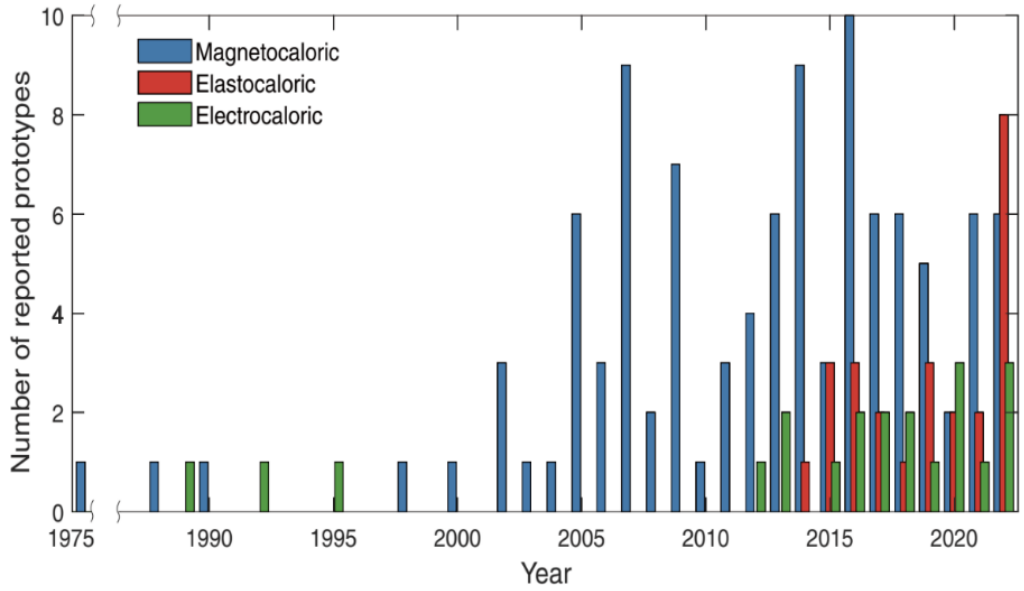

Figure 1.2. Prototypes are developed per year for solid-state cooling technologies [32].

1.4 Elastocaloric effect

A number of publications based on the elastocaloric effect (eCE) are presented in Figure 1.3. It shows that most studies focus on the fabrication of materials and their performance analysis. Then, the experimental and modeling-based research is done.

1.4.1 Elastocaloric working principle

The eCE is the application of unidirectional mechanical stress under adiabatic conditions to a solid eC material. It is based on the reverse Brayton cycle. As shown in Figure 1.4, eC cooling consists of four steps. First, an adiabatic load on the eC material is applied, which increases the temperature of the material rejected by the sink when the applied load is kept constant for some time. In the second step, which leads to a temperature decrease, unload the material temperature below the temperature of the first step.

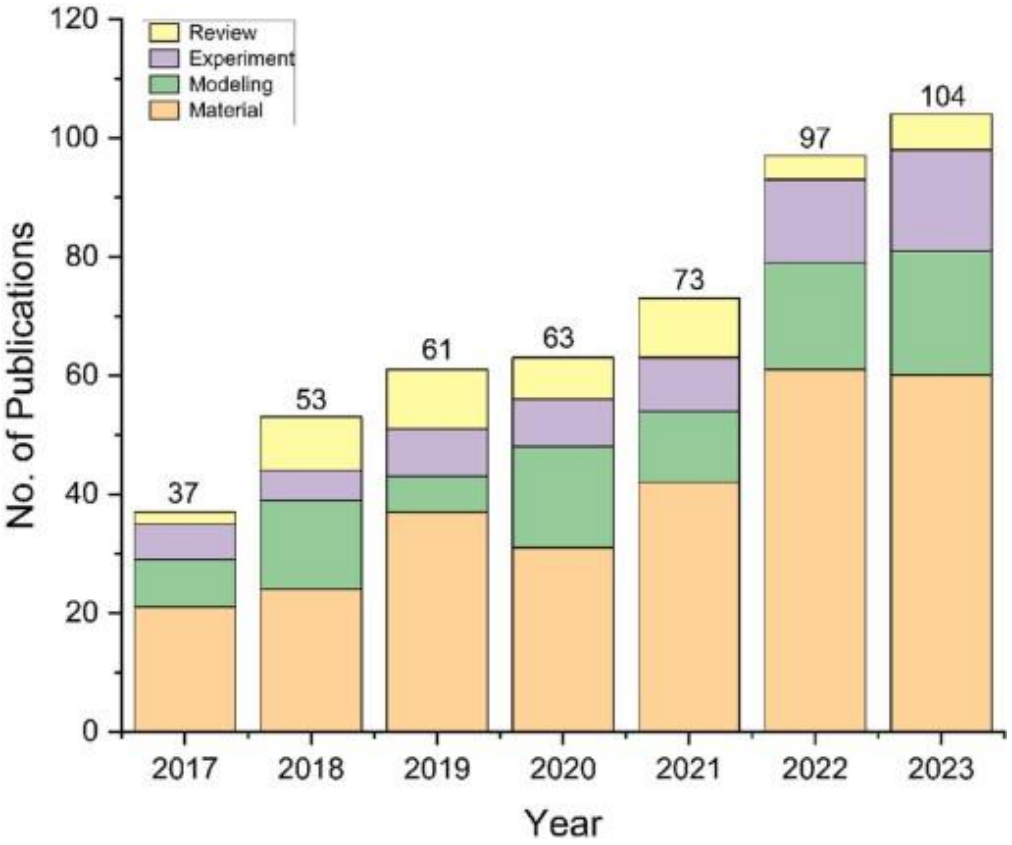

Fig. 1.3. Number of publications for eC [33].

Finally, the unloading is maintained for some time, and the material's surface is brought in contact with the source material, ultimately leading to the material's cooling. The eCE leverages stress-induced phase transformations in materials (e.g., shape memory alloys like NiTi) to achieve cooling via a reverse Brayton cycle. Here is a detailed breakdown of the four-step process:

(i) Adiabatic loading (phase transformation + heating): A mechanical stress (tension or compression) is rapidly applied to an eC material. It triggers a transition from the austenite phase to the martensite phase. This transformation is accompanied by the release of latent heat, making the process exothermic. As a result, the temperature of the material rises significantly; for example, in NiTi, the temperature increases by 25 K.

(ii) Isothermal heat rejection (cooling to sink): After the initial loading, the applied stress is held constant to transfer heat to the sink, such as ambient air or a coolant. During this stage, the material remains in the martensitic phase while its temperature gradually decreases and approaches the initial temperature. The efficiency and speed of this cooling process depend on the material’s thermal conductivity and the effectiveness of the heat exchanger design employed to remove the heat.

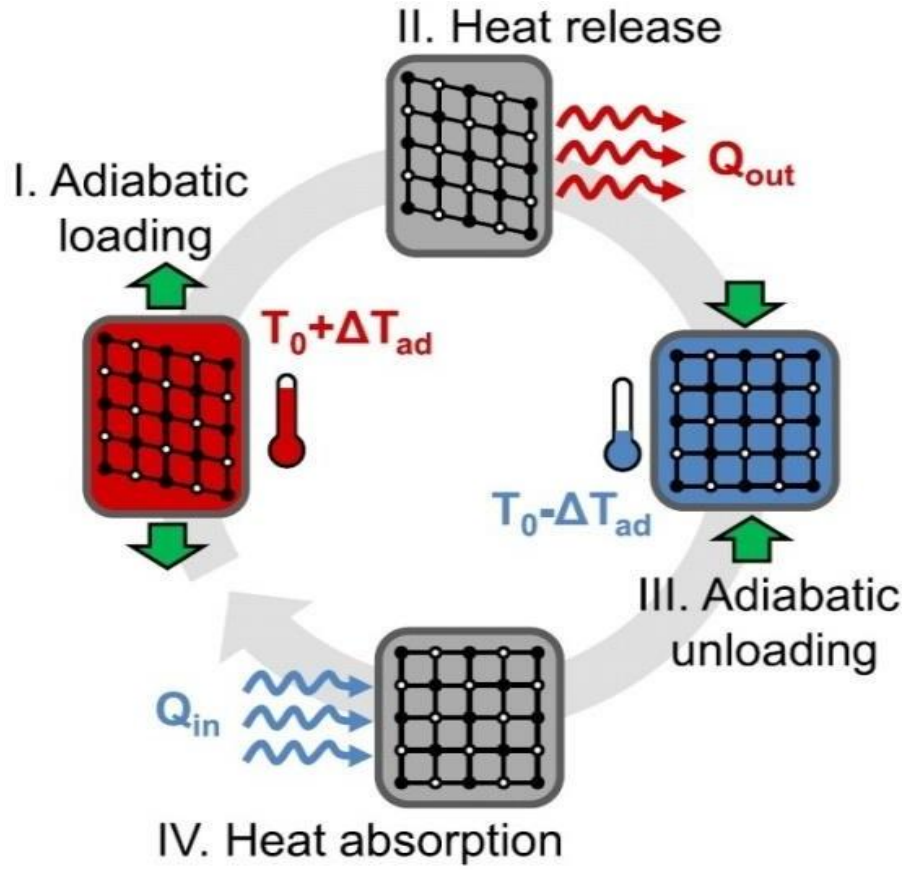

Figure 1.4. Schematic diagram showing the working of eCE material upon application of the electric field [5].

(iii) Adiabatic unloading (reverse phase transformation+cooling): Applied stress is rapidly removed, and the material undergoes a reverse phase transformation from martensite to austenite. This process is endothermic and absorbs heat from the material's surroundings. Thus, the temperature of the material drops, often falling below its original starting point; for instance, NiTi wires can experience a temperature decrease of around 21 K.

(iv) Isothermal heat absorption (cooling the source): After unloading, the material is kept unstressed, allowing it to absorb heat from the surrounding environment or the target cooling space. During this phase, the material gradually warms to its original temperature, completing the eC cooling cycle and preparing it for the next loading stage.

1.4.2 Elastocaloric materials

Materials are a major constituent of eC technology; it is necessary to know the material's performance under different conditions, costs, and life to be operational for cooling applications. The eCE was observed in materials like rubber, metals, and wood in the 19th century under a mechanical load cycle at room temperature [35, 36]. The development in eC refrigeration has been very recent since 2012 due to dominant refrigeration and cooling technology based on vapor compression. The materials reported for eC cooling are shape-memory alloys

(SMA), shape-memory polymers, natural rubber [30], ferroelectric ceramics [27], etc. The eC materials are expected to produce high adiabatic temperature change or high isothermal entropy change, or high latent heat with an input of a small amount of mechanical work. It should possess high thermal conductivity and other material properties should not change over a large temperature range [37]. Further, it must have a high fatigue life to withstand millions of load cycles without functional or structural degradation. Among the reported eC materials, natural rubber and shape memory alloys are most explored due to ease of availability, low cost, and higher fatigue life. The various categories of the eC materials are discussed below:

(i) Shape memory alloys (SMAs): These metals can change their internal structure when stressed, resulting in a temperature change. Examples include nickel-titanium (NiTi), copper-based alloys (like Cu-Zn-Al), and iron-based alloys. They are known for their strong cooling effect and durability.

(ii) Elastocaloric polymers: Some flexible plastics, such as natural rubber and specially designed elastomers, can also show a cooling effect when stretched and released. They generally require less force than metals and are valued for their flexibility.

(iii) Shape memory polymers (SMPs): These are engineered plastics that can return to their original shape after deforming and exhibit temperature changes under mechanical loading. While their cooling effect is usually smaller than metal alloys, they are lightweight and adaptable.

(iv) Other materials: A few ceramics and certain magnetic materials have also shown eC behavior, though they are less common in practical cooling devices. SMAs are the most extensively applied eC materials due to their superelastic properties, shape memory, and superelasticity. Figure 1.5 has been discussed below:

(a) Strain vs. temperature diagram

The SMAs under stretching varies in temperature because the material's internal structure changes from austenite to martensite. This transformation releases heat; Figure 1.5(a) shows an upward jump in temperature as strain increases. The process reverses if the stress is released: the material cools down, even dropping below its original temperature. This heating and cooling cycle is the essence of the eCE.

(b) Stress vs. strain diagram

The force (stress) applied against material stretches (strain) will show an initial straight line; see Figure 1.5(b). This is the elastic region. As it keeps pulling, the curve flattens into a plateau, meaning the material changes phase at nearly constant force. Once the transformation is complete, the curve rises again. A hysteresis loop shows some energy lost in each cycle when the path does not retrace exactly.

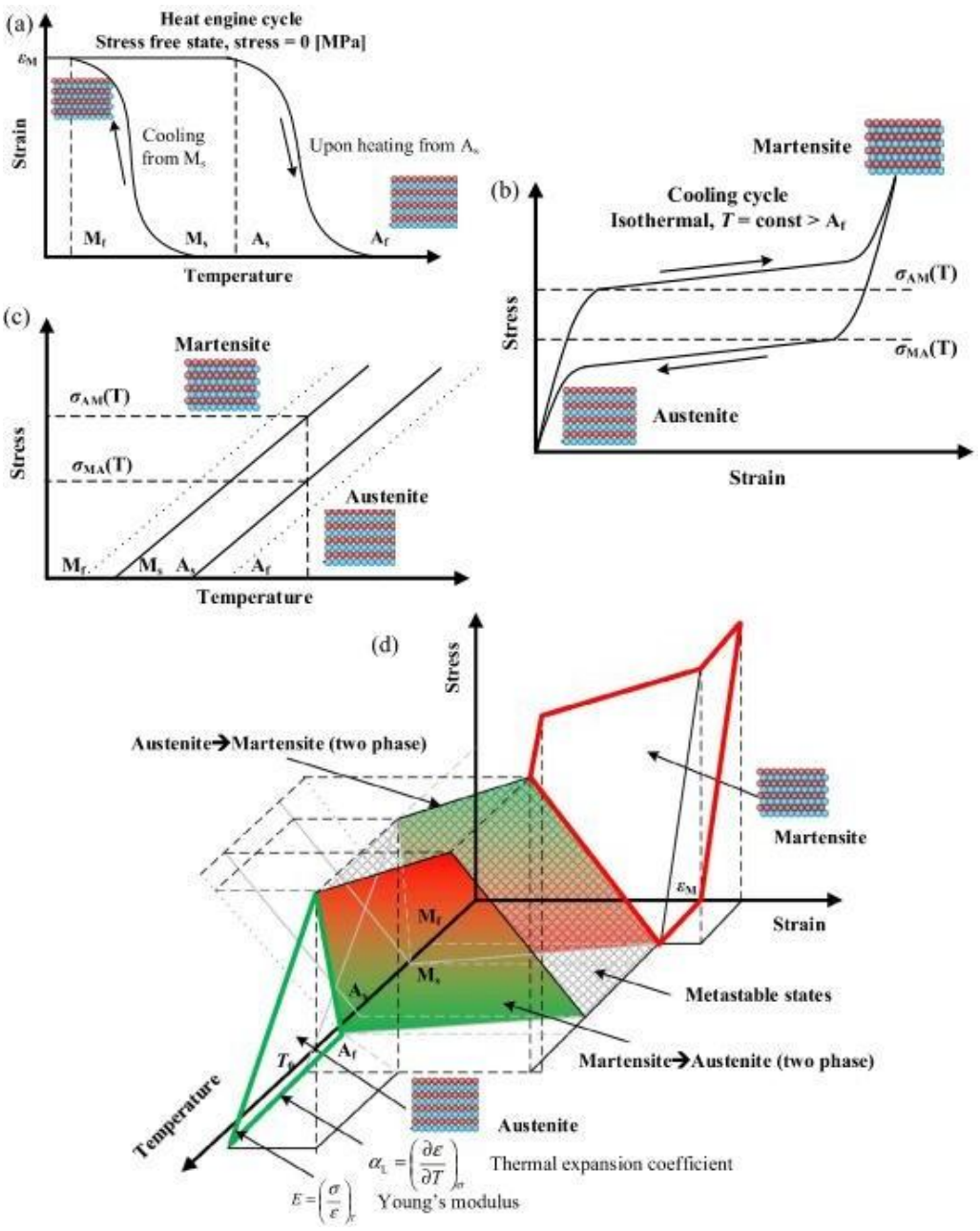

Figure 1.5. A visual summary of eC material characteristics: (a) Temperature hysteresis loop (b) Hysteresis between stress and temperature (c) Constitutive relationship depiction (d) Three-dimensional phase diagram [38].

(c) Stress vs. temperature diagram

Figure 1.5(c) shows the force needed to cause the phase change at different temperatures. As the temperature increases, more force is needed to trigger the transformation. This relationship is important for designing cooling systems, as it defines the range of temperatures where the eCE can be operated efficiently.

(d) Stress-strain-temperature diagram

Figure 1.5(d) shows all three factors interact: apply more force at a specific temperature, and the material stretches and heats up due to the phase change. This visualization helps engineers understand and optimize how SMAs behave in real cooling devices, making it easier to design systems that take full advantage of the eCE.

1.5 Research Objectives

This work focuses on eCE to solve the problem of high-temperature electronic LED cooling. The performance of the eCE device is investigated with the following objectives:

1. Tensile or compressive stress is applied to obtain phase transformation and validate results.
2. Effect of various parameters on the eC cooling.
3. Modeling the heat transfer domain for obtaining temperature cycles.
4. Modeling the eC materials for the cooling of electronic components.

1.6 Thesis Structure

The thesis is organized into five comprehensive chapters that collectively address the development and application of eC cooling for automotive LED headlamps. It opens with a detailed introduction that sets the context by discussing the limitations of conventional cooling technologies, especially in compact and energy-sensitive applications. Chapter 1 thoroughly classifies various traditional and emerging cooling methods, particularly solid-state cooling. Then, it narrows the focus to the eCE, explaining its working principle and material considerations. Research objectives are laid out to frame the study’s scope and direction.

Chapter 2 elaborates on the modeling methodology, detailing the equation-based approach employed to simulate eC behavior and how COMSOL Multiphysics was employed to design and validate the cooling mechanism. Chapter 3 presents the validation of these models by comparing simulation results with existing experimental data, focusing on the materials' stress-strain behavior and temperature change profiles. In Chapter 4, the thesis explores the practical application of the eCE for LED chip cooling, analyzing its performance relative to conventional methods like heat sinks and forced air cooling. The final chapter 5 concludes the findings and suggests future research avenues, including improvements in material design and integration into real-world automotive systems.

Chapter 2

Methodology and Modeling

This chapter describes the equation-based modeling to estimate the elastocaloric effect (eCE). It utilizes heat accumulation-based relations, whereas the model should employ caloric relations. Initially, equation-based modeling analyzes the eCE and validates the model with the literature. The built-in eC module was unavailable in COMSOL. Thus, eCE and stress vs strain validation were verify the modeling. The results suggest that any equation-based modeling can be employed for eC analysis.

2.1 Introduction

Several simulation methods can predict the material's elastocaloric (eC) potential; these simulations are also available with various designs for the heat source and heat sink. Also, the experimental validation for these simulation results based on the temperature cycles is done. However, the design for a particular application has been explored less. The eCE is explored in the literature for different strain rates, stress values, fatigue life, etc. In this direction, Ossmer *et al.* [39, 40] experimented and validated the temperature profile using a simulation using a phenomenological Tanaka-type model, where the mechanical and thermal equations were solved using COMSOL Multiphysics. Tusek *et al.* [41] trained at different temperatures for isothermal and adiabatic testing. Vladimir *et al.* [42] applied Monte Carlo simulations for thermal hysteresis in Heusler alloys. Bingfei *et al.* [43] considered molecular dynamics simulations for thermal cycling and porosity effects on phase transformation in porous nanocrystalline SMA. The research revealed that the phase transformation capability is reduced as porosity increases and the number of cycles.

To increase eC cooling efficiency, Nora *et al.* [44] presented a MATLAB-Simulink simulation model that utilizes an active eC heat pipe, achieving 67% material efficiency by mitigating thermal losses and hysteresis, which highlights eC cooling's potential as a sustainable, high-performance alternative to traditional refrigerants. Also, previously [45], a phenomenological model was employed to determine the eCE for first-order eC materials. It considers adiabatic temperature change, strain, dissipative energy, and heat capacity as a function of temperature and stress. Yanliang *et al.* [46] reported a compact standalone eC refrigerator using polycrystalline NiTi wires that achieves a 20% higher volumetric specific cooling power and a 9.2 K temperature span, with 3.1 W cooling power sufficient for a 0.9-litre compartment. Replacing wires with NiTi plates could boost cooling power to 17.9 W, demonstrating strong potential for space-saving, eco-friendly cooling in small appliances. Xueshi *et al.* [47] designed a compact eC air cooler using NiTi sheets that achieves a 5.5 K temperature drop with a specific driving force of 5.64 N/g-100*x* lower than previous tension/compression-based systems

employing air as the heat-transfer fluid, eliminates bulky heat exchangers, enabling a compact design. The device delivers 11.5 W cooling power and shows potential for scaling to 1 kW with a 40 kN actuator, highlighting feasibility for commercial low-force cooling applications. In an attempt to present the first demonstrator from Italy, Luca *et al.* [48, 49] applied COMSOL Multiphysics and MATLAB code for a finite-element method for numerical optimization of a single bunch of shape memory alloy (SMA) wires for eC model preparation. A small eC device using NiTi wires and air as the heat transfer fluid was tested for electronic circuit cooling, comparing tensile and bending load methods. The tensile configuration achieved a higher maximum temperature span (9 K vs. 7.2 K) and cooling power (76 W vs. 65 W). However, the bending configuration consistently showed a much higher COP, making it more energy-efficient and promising for compact electronics cooling. The eCE computational equation-based mathematical modeling in COMSOL Multiphysics software is discussed here. As the present COMSOL software does not have a module for modeling the eCE, the heat transfer and solid mechanics module is considered for modeling. Further, the laminar flow is applied to study multiphysics using non-isothermal flow. The model is validated with literature before moving further with the application of eCE.

2.2 Equation-based modelling

The eCE is a reversible temperature change under adiabatic conditions or isothermal change in entropy when a stress or strain is applied or removed from an eC material, as shown in Figure 1.4. The internal energy change per unit volume, as per the first law of thermodynamics, is given by

$$dU = dQ + dW \tag{2.1}$$

where U denotes the system's internal energy, Q represents heat absorbed, and W is the work done on the system. Also, as per the second law of thermodynamics, for a reversible process, the heat absorbed by the system is given as:

$$dQ = TdS \tag{2.2}$$

where T is absolute temperature, and S is entropy. The amount of hysteretic work required for driving the eC work is given by

$$dW = \sigma d\varepsilon \tag{2.3}$$

where σ is the amount of stress applied and ε is the strain developed in the material. The Gibbs free energy from the above equations is given as:

$$G = U - TS - \sigma\varepsilon \tag{2.4}$$

where G is the Gibbs energy. The critical stresses (σ) for forward and reverse phase transformations in superelastic SMAs increase linearly with temperature, governed by the Clausius-Clapeyron relation:

$$\frac{\partial \sigma}{\partial T} = \frac{\partial S}{\partial \varepsilon_T} = \frac{\Delta H}{\varepsilon_t T} \tag{2.5}$$

where ΔS is entropy change and ε_t is transformation strain. This linear dependence ensures phase transitions occur without irreversible damage when applied stress exceeds σ_1 but remains below the austenite's yield stress. When the differential form is converted into the integral form during a quasi-static process, the isothermal entropy (ΔS):

$$\Delta S = -\int_{\sigma_0}^{\sigma_1} \left(\frac{\partial \varepsilon}{\partial T}\right)_{\sigma} d\sigma \tag{2.6}$$

From the entropy change, the temperature change is obtained as:

$$\Delta T = -\int_{\sigma_0}^{\sigma_1} \frac{T}{C} \left(\frac{\partial \varepsilon}{\partial T}\right)_{\sigma} d\sigma \tag{2.7}$$

As the eCE is a phenomenon that causes temperature change, the basic heat transfer equation in a differential form, which is available in COMSOL, as

$$\rho C_p \left(\frac{\partial T}{\partial t}\right) + \rho C_p u.\nabla T + \nabla.q = Q + Q_{ted} \tag{2.8}$$

where ρ is the density of the material, T is the temperature, and C_p is the material's heat capacity. Also, $q = -k\nabla T$ where k is the material's thermal conductivity, ∇q is the term corresponding to conductive heat transfer, $\rho C_p u.\nabla T$ represents convective heat transfer, and Q_{ted} represents thermoelastic damping, which can also be neglected ($Q_{ted} = 0$). Hence, equation 2.8 can be rewritten as,

$$\rho C_p \left(\frac{\partial T}{\partial t}\right) - k\nabla^2 T = Q \tag{2.9}$$

where Q is the heat source and the amount of latent heat the material possesses. It can also be modeled in the form of stress:

$$Q = -\rho T \frac{\partial S}{\partial \sigma}\frac{\partial \sigma}{\partial t} \tag{2.10}$$

The temperature change by eCE results in the entropy of the material due to stress(σ) obtained by

$$S_1 = C_1\sigma^2 + C_2\sigma \tag{2.11}$$

where C_1 and C_2 are constants. The above equation is applied to fit entropy as a function of stress. Hence, the combined equation is written as:

$$\rho C_p \left(\frac{\partial T}{\partial t}\right) - k\nabla^2 T = -\rho T \frac{\partial S}{\partial \sigma}\frac{\partial \sigma}{\partial t} \tag{2.12}$$

Further, by solving the above equation, the eC $\frac{\partial T}{\partial t}$ can be obtained. However, the entropy obtained depends on coefficients C_1 and C_2, which depend on stress variation. Hence, the above equation concerning the material involved and applied stress is limited. Therefore, an alternate modeling approach can be adopted where temperature change can be derived in terms of the latent heat of the material.

The adiabatic temperature change can be evaluated using the isothermal entropy change and the latent heat of transformation, $Q_{\text{lat.}}$

$$\Delta T_{\text{ad}} = \frac{-Q_{lat}}{C_p} \tag{2.13}$$

where Q_{lat} can be modeled as $T\Delta S_{iso}$. Hence, the latent heat during the phase transformation can be obtained using the DSC, which is thermally induced, although phase transformation for an eC cycle is stress-induced. It is important to note that the stress-induced transformation is a fraction of the latent heat Q_{lat} of the thermally induced phase transformation. A time-dependent simulation is carried out in COMSOL Multiphysics. The detailed explanation of the modeling in COMSOL is discussed further for better understanding. The step-by-step modeling procedure is discussed in section 2.3. A stationary solver is used to validate the stress-strain curve.

Table 2.1. Properties of NiTi shape memory material [40].

Property	**NiTi**	**Unit**
Poisson's ratio	0.33	-
Density	6500	Kg/m^3
Thermal conductivity	18	W/(m.K)
Martensite start temperature	252	K
Martensite finish temperature	241	K
Austenite start temperature	289	K
Austenite finish temperature	301	K
The slope of the martensite limit curve	$5.7*10^6$	Pa/K
The slope of the austenite limit curve	$5.7*10^6$	Pa/K
Young's Modulus Austenite	$25*10^9$	Pa
Young's Modulus Martensite	$25*10^9$	Pa
Heat capacity at constant pressure (Austenite)	500	J/(kg.K)
Heat capacity at constant pressure (Martensite)	500	J/(kg.K)

2.3 COMSOL Modelling

The eCE stress-strain diagram is validated in COMSOL Multiphysics using solid mechanics and a stationary study. Further, a time-dependent study validates temperature vs time using solid mechanics and heat transfer in solids modules. These modules are chosen from the COMSOL Multiphysics software's initial interface. The modeling procedure is further discussed in detail in Figure 2.1. In order to understand the modeling, firstly, define the basic parameters required in the simulation in the parameters tab, which is present in the model builder in the

upper left side of COMSOL software; defined values like maximum stress, reference temperatures, and or dimensions of the geometry. In Figure 2.1, Component 1 contains a definition tab comprising various functions. The stress is varied with time using interpolation or piecewise functions. As a result, the stress is applied using these functions, and the stress vs strain or temperature vs time profile is obtained using boundary conditions.

It is observed that the values of stress, loading/unloading time, and operating temperature affect the curve of stress-strain and temperature profile, which is further discussed in detail in Chapter 3. The trial-and-error method optimizes the cycle to obtain temperature and stress diagrams. In order to obtain the stress-strain curve, an interpolation function is employed along with an analytic function. It makes the interpolation function periodic by defining the periodicity time in the periodic extension section in the settings of the analytic function. Similarly, interpolation and analytic functions are considered to obtain the temperature profile. Instead of an interpolation function, a piecewise function can be considered in which the functions depend on time. A function is created by entering starting and ending point values using a piecewise function. The parameter t needs to be defined, which is time; the cycle is made periodically using extrapolation options to define the setting in the piecewise function. Smoothing can smooth the endpoints if there is a sharp change in the direction, which may lead to failure in convergence at the point. While validating the stress-strain diagram, smoothing is not applied. Smoothing can be applied with relative size in the transition zone as 0.001, where the smaller transition zone implies that the curved points are smoother. This may lead to increased computing time.

In the current study, the source and sink temperatures need to be monitored, which can be estimated using a domain probe from the probe list in the definition section of the model builder section of COMSOL. Hence, a domain probe is selected, displaying a temperature (K) vs. time (s) graph, allowing viewing of the adiabatic temperature change. All representation-related options can be configured in the display tab, including geometry labels, grid, axis orientation, axis units, etc.

Figure 2.1 shows the geometry 1 tab as the next step to the component, where geometry is defined using various shapes. In this study, a heat sink with a rectangular chip that needs to be cooled is utilized. A cuboidal-shaped NiTi material between the heat sink and chip source is considered. The dimensions of NiTi material are 17×17×1 mm^3. The chip material to be cooled has dimensions of 15×15×2 mm^3. An air domain with dimensions 70 x 30 x 15 (mm^3) has been considered and the inlet and outlet of airflow are defined. Once a rectangular block in geometry is selected, all the dimensions are entered in the size and shape section, which is present in the settings. The dimensions are adjusted as per analysis requirements. The block's position can change based on the geometrical structure at the corner or the center, with changing values of *x*, *y*, and *z* directions. Coordinate systems can also be specified in work planes, such as *xy* or *yz*.

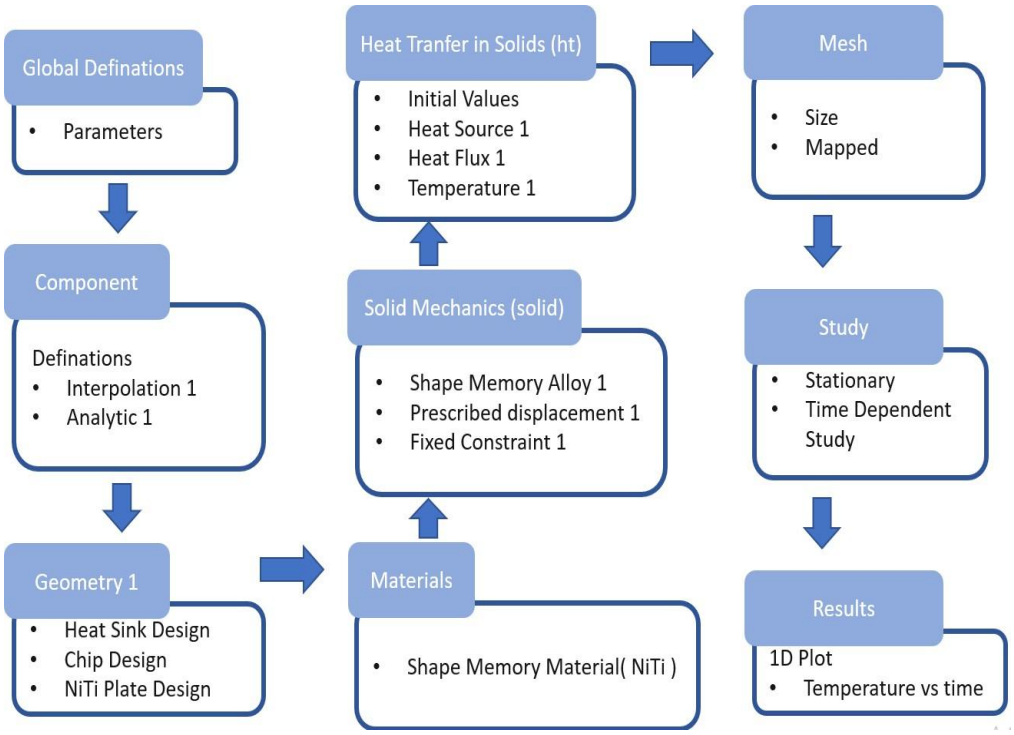

Figure 2.1 Detailed information about COMSOL modeling.

As shown in Figure 2.1, materials are to be specified for the respective geometries. In order to specify the material, add an in-built material from the already present library, which includes all the necessary material properties. However, if the same is unavailable, it can add blank material, and values can be entered manually in the property table. It is to be noted that a material is assigned to each geometric part in order to avoid errors. The material properties for NiTi are utilized from Table 2.1, and other properties like silicon for the chip, aluminum for the sink, and air for the air domain are made from the inbuilt materials. The eCE is based on the idea that providing stress or strain on material and unloading the material with an adjusted holding time between loading and unloading leads to the absorption and release of heat, respectively. In this study, the solid mechanics module is operated to apply the stress field and to get temperature cycles. The heat transfer in the solids module is discussed further. Specify boundary conditions based on the physics study after assigning the material to the respective geometries. Here, the solid mechanics module obtains the temperature profile concerning time using the heat transfer in the solids module. In solid mechanics, a prescribed displacement is applied to the stress on one end of the geometry using interpolation and an analytic function defined in the definition section. Secondly, a fixed constraint on the opposite side of the prescribed displacement on the cuboidal geometry is considered, as shown in Figure 2.2. In the solid mechanics module, shape memory alloy SMA material exhibits superelasticity and shape memory properties.

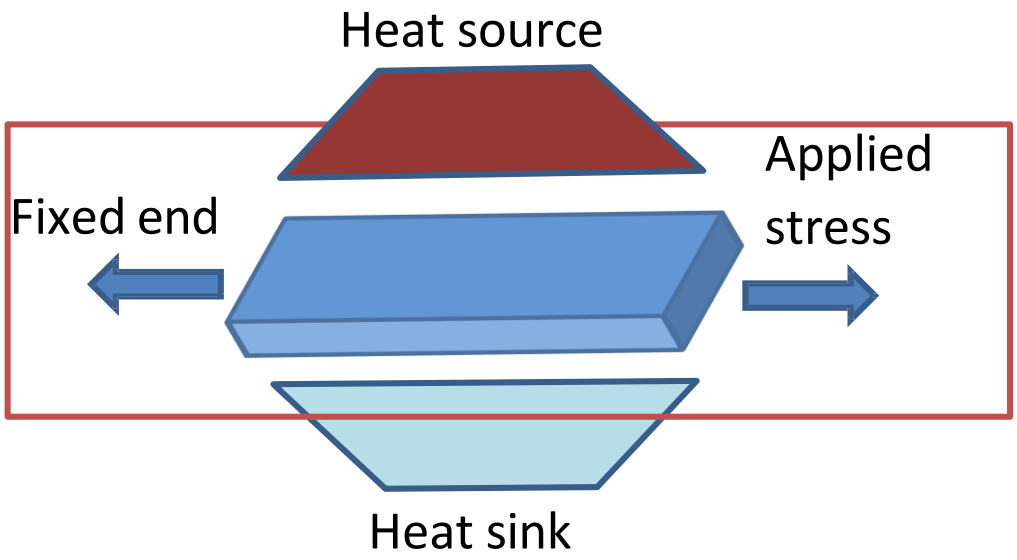

Figure 2.2 Schematic representation of an eC device.

In shape memory alloy, the temperature is considered as ambient temperature as 293.15 K, and the material model is Lagoudas, with all the properties extracted from the material specified. In the energy dissipation section, the dissipated energy is calculated. Further, heat transfer is modeled in solids is considered as depicted in Figure 2.1. The heat transfer is applied to obtain temperature cycles concerning time. This module's initial temperature was 293.15 K. A heat source was modeled with a general source and a specified total power dissipation density (solid). Instead of this, the latent heat value can be defined in the heat source under user-defined conditions. Further, heat flux has been given to one of the surfaces through which the geometry is exposed to the surroundings, while convective heat flux is taken as the flux type in the heat flux section in settings. The heat transfer coefficient is 120 W/m^2K after analysis of various values at an ambient external temperature of 293.15 K. The heat transfer in the solids and fluids module is considered to apply the temperature cycles obtained from the discussed study for the application part using a heat source and heat sink; see the schematic in Figure 2.2.

After the model was prepared, the meshing used user-controlled standard mesh or mapped mesh to generate a map to a regular grid on a 2D domain and 3D boundaries. A triangular mesh was made on one of the surfaces and swept over the entire geometry as per the requirement in the geometries. In order to study, the stationary and time-dependent studies have been considered. The start and end times need to be defined, and the tolerance needs to be specified as physically controlled or user-defined values. The tolerance needs to be changed depending on errors and the requirement for the result. The values that are too high and low might create errors in the simulation or not give accurate solutions. Finally, various plots are available as per default plots generation defined in study settings, or plot various other results according to the domain probe defined in

the definition section earlier; also, 1D, 2D, etc, plots are available, which help us plot other values not already defined.

2.4 Automotive LED cooling using a heat pipe.

The current technology used for automotive headlight cooling dominantly utilizes either a heat sink or a combination of a heat sink with a fan. However, a heat pipe and cooling fan are applied in modern high-power LEDs, as shown in Figure 2.3. Although our focus in this study is not on high-power headlight cooling, it is on integrating eCE for cooling the LED operated for the low-power light guide present in the headlight found in the upper part of the headlight.

2.5 Conclusion

This chapter considers a mathematical methodology to describe eCE modeling. Equation-based modeling mathematically depicts the eCE, which discusses how phase transformation in shape memory alloys can lead to cooling cycles. The Clausius-Clapeyron equations are applied to obtain temperature change. The schematic discusses how, following a particular procedure, the eCE can be modeled in COMSOL Multiphysics. Although an inbuilt model for eC is not available currently, it is expected to be available in the future; it will be interesting to compare the developed and the inbuilt models. COMSOL Multiphysics modeling provides a solid foundation for further investigation of eCE in detail in the following chapter for validation and application of eCE.

Figure 2.3 Heat pipe and fan cooling combination used for headlight cooling [50].

Chapter 3

Validation

This chapter describes various validations before proceeding with the application of the eCE. Although the eC module is not available in COMSOL, the simulation approach is utilized in COMSOL Multiphysics, using mathematical equations, solid mechanics, and heat transfer modules to validate the simulation and experimental results. In this chapter, SMA's phase transformation defies the criteria for obtaining the stress and temperature cycles.

3.1 Introduction

In the past decade, eCE has been determined in various materials and proposed for eC cooling devices. Optimizing existing approaches, such as studying the impact of varying the loading stress or strain, holding time, and temperature at which it can be operated, are important factors. Most of the research is focused on shape memory alloys due to their properties, like shape memory and superelasticity. In this chapter, the validations are discussed to apply the eC design for cooling applications in Chapter 4. The validation of stress-strain hysteresis is discussed in detail in 3.2. Segment 3.3 discusses temperature cycle validation and variation of constants in order to obtain the highest and lowest temperatures in the austenite and martensite phases. Finally, the curves obtained are compared with the temperature vs time curves from previous research in section 3.4.

3.2 Stress-strain diagram validation

The first step in the study is a validation of the stress-strain curve. In SMA's, the curve is not a single line curve but instead includes hysteresis, which is due to the phase transformation in the material due to phase change associated with the applied stress values. The loading and unloading rate has also varied, along with the change in stress values. Also, the variation of holding time has been examined; hence, the stress-strain diagram is validated by Ossmer *et al.* [40]. The NiTi material considered in this study is initially in the austenite phase. When a certain amount of stress is applied, the material undergoes phase transformation, and the high-temperature phase austenite has a higher symmetry lattice structure transforms to a low-temperature martensite phase. Due to the lower symmetry of the martensite structure, one austenite structure can transform into 24 variants of martensite, which have the same crystal structure but differ in orientation. The austenite phase transformation starts at the austenite start temperature, $A_{s,}$ and completes at the austenite finish temperature, $A_{f,}$ during heating of the SMA. Also, the martensite phase transformation starts at martensite start temperature M_s and martensite finish temperature M_f during the cooling of the SMA. The amount of work for eC cooling is the area enclosed by the material's stress-strain

curve during the loading cycle. The representation of the eCE depends totally on thermal boundary conditions while loading and unloading. The properties of SMAs are critical stresses for transformation from austenite to martensite, martensite to austenite, and transformation strain.

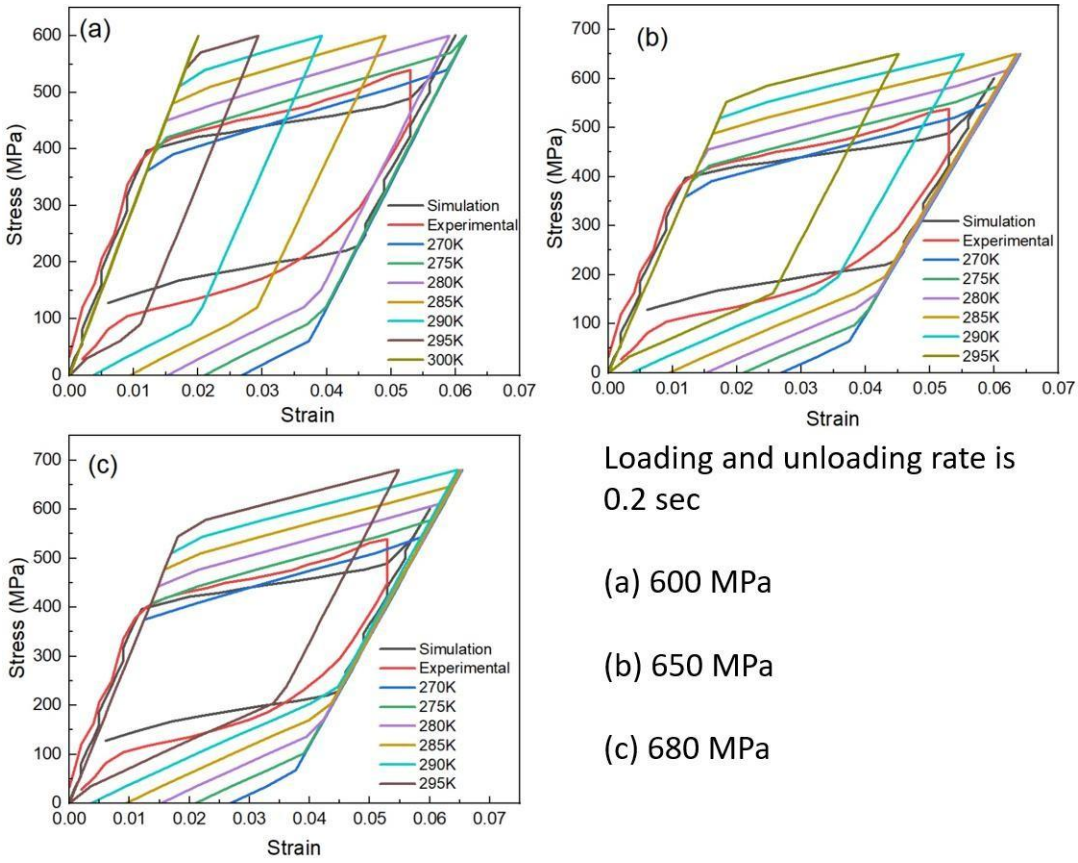

Figure 3.1 Strain-strain graph for different values of stress and the same loading-unloading rate.

Figure 3.1 shows a three-dimensional model having dimensions 15mm x 2mm x 20µm made by Ossmer *et al.* [40] with the properties given in Table 2.1, which has been simulated using COMSOL Multiphysics. The same time value for loading and unloading the material, i.e., 0.2 seconds, is considered. Variations have also been made concerning temperature and stress values. A solid mechanics module and a stationary study to simulation are considered. A trapezoidal curve is applied with the help of a piecewise function where start and end values of the parameter and a function value are specified. The stress is defined in the parameters section. The boundary load is selected to specify the function in the solid mechanics section. A fixed constraint is selected to fix the opposite end. Figure 3.1 presents a higher operating temperature; the strain value decreases for similar stress. At 600 MPa, 650 MPa, and 680 MPa, the loading curve is close to the simulation and experimental results at 270 K.

The validation is further done for different loading and unloading times, as shown in Figure 3.2, where the loading time is kept at 0.02 seconds and the time for unloading is 0.2 seconds. The variation is done with 550 MPa, 600 MPa, and 680

MPa at different temperatures is depicted in Figure 3.2. For higher temperatures, the curve deviates from the experimental and simulation results of Ossmer *et al.* [40].

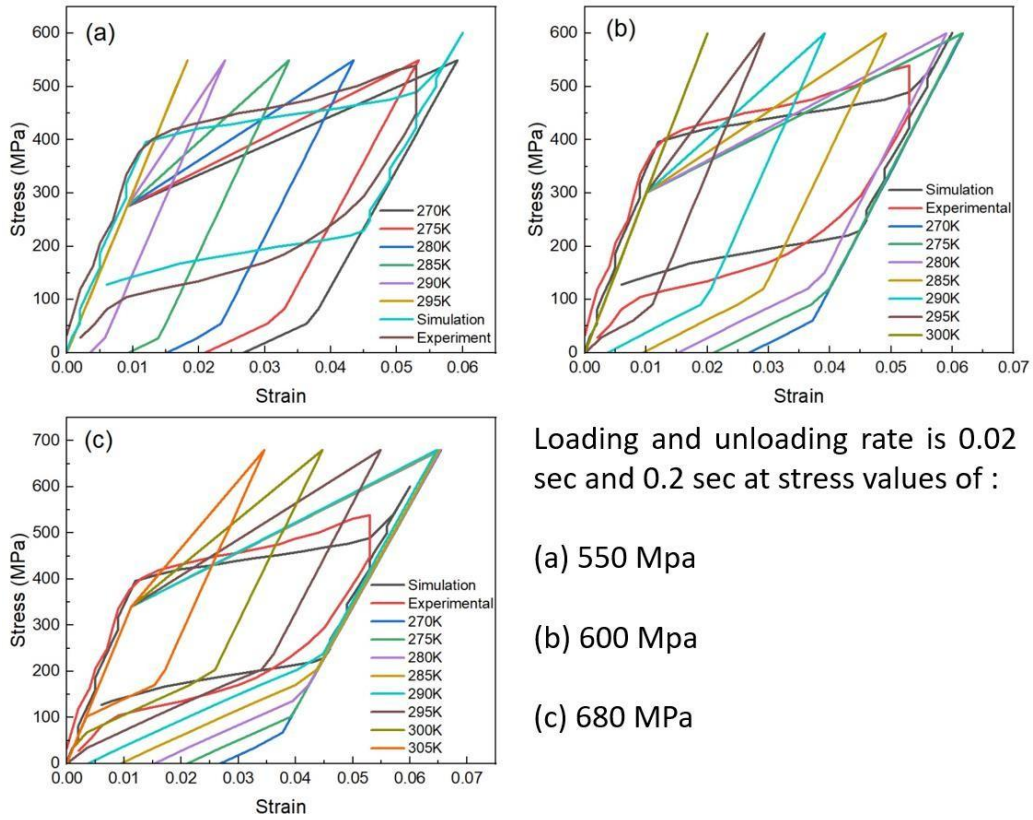

Figure 3.2 Strain-strain graph for different stress with various loading and unloading rates.

Figures 3.1 and 3.2 clearly show that the model variation needs to be done concerning the loading and unloading rate for validating the stress-strain diagram. Hence, 0.03 seconds loading time and 0.02 seconds unloading time have been applied for 600 MPa, which is close to the simulation and experimental data from Ossmer *et al.* [40] see Figure 3.3. Although the model is still deviating in the lower region, the exact mathematical equation could not be employed, as mentioned in the paper. The validation also mentions the operating temperature as 280 K. Once the stress is applied, the SMA is initially in the austenite state and transforms into the martensite phase. A detailed explanation of the behavior of the SMA for eC cooling is discussed here.

Shape memory alloys (SMAs) show distinctive stress-strain behavior crucial for eC cooling. Initially, they deform elastically in the austenite phase with a linear stress-strain relationship. When stress reaches a critical level, the SMA transforms into martensite at nearly constant stress, releasing latent heat and causing a temperature rise. Further stress leads to elastic deformation of martensite, but excessive strain can cause permanent damage. Upon unloading, the reverse transformation back to austenite absorbs heat, producing a cooling effect.

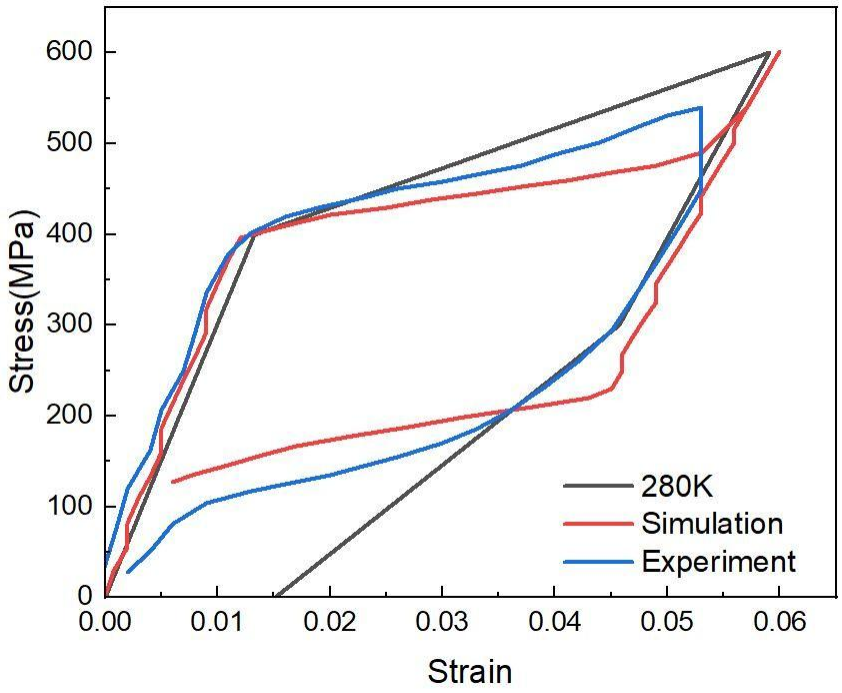

Figure 3.3 Stress-strain validation graph.

This loading-unloading cycle forms a hysteresis loop, representing energy loss that affects efficiency. Key factors influencing cooling performance include transformation strain, hysteresis width, and strain rate. Materials with narrow hysteresis and high recoverable strain yield better cooling. Innovations like additive manufacturing improve material properties while bending actuation reduces driving force requirements. These advances make SMAs a promising, energy-efficient alternative for sustainable cooling technologies.

3.3 ECE validation using stress equation

The temperature validation is done separately for the austenite and martensite phases by equations discussed in Chapter 2.2. The Landau theory approach is exercised along with the entropy equation in the form of stress values, which also depend on the constants C_1 and C_2 utilized for a 600 MPa. Figures 3.4 and 3.5 also mention values of C_1 and C_2. As entropy is a function of stress, a change in entropy is associated with a temperature change. However, the austenite and martensite phases cannot be simulated simultaneously using these assumptions; hence, validation of the austenite and martensite phase temperature change values has been done separately. Figure 3.4 presents the temperature change of the austenite phase using Landau theory in COMSOL Multiphysics. In the process, the values of C_1 and C_2 have been specified, keeping the stress at 600 MPa. The parameters are defined in the parameter section. Material properties of the austenite phase are specified in the materials section. A piecewise function is defined as a function of loading and unloading times. A piecewise function defines the stress, and the stress value is given in the parameters section. The variable function defines the stress as a function of time, with time as stress = stress(t).

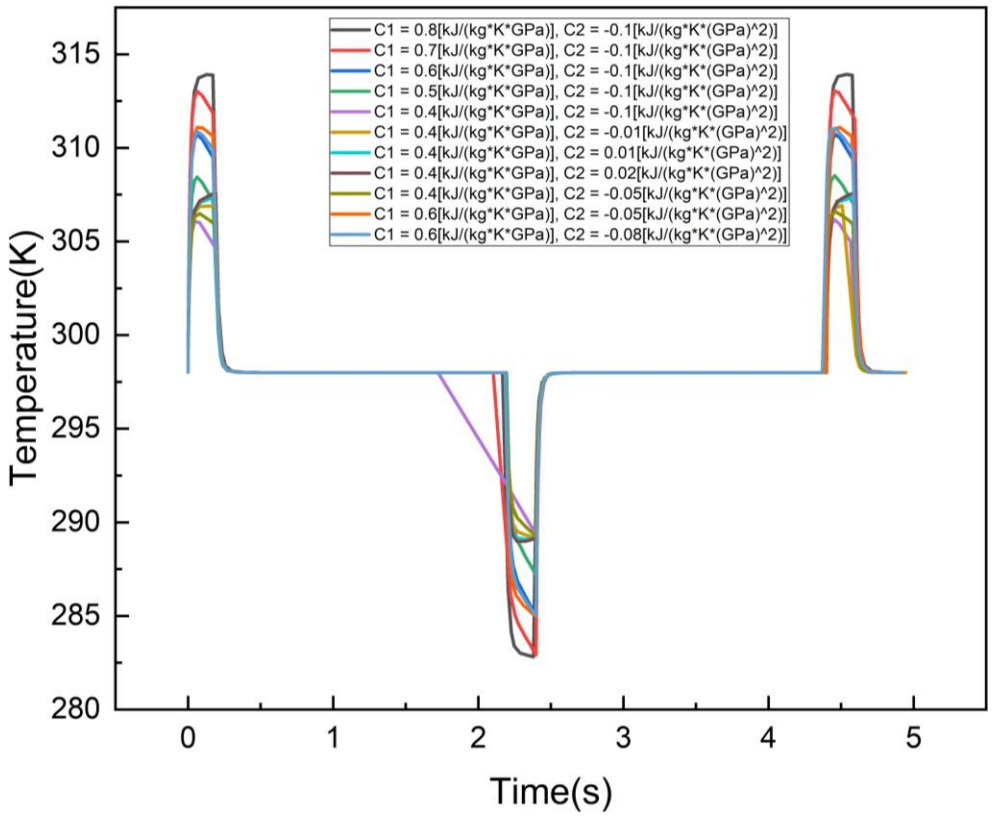

Figure 3.4 Temperature time-varying values of C_1 and C_2 in the stress equation for the austenite phase.

Also, the entropy value is defined as the stress function, as mentioned in equation 2.11. The solid mechanics module and the heat transfer in the solids module in COMSOL are employed. The solid mechanics module utilizes boundary conditions and boundary loads to apply the load on one end of the geometry, and a fixed constraint was applied on the opposite end. The heat transfer module considers equation 2.12 for modeling the heat transfer as a function of stress in the heat source, and shape memory alloy is selected for the geometry as Q = rho×T×d(S, stress)×d(stress,t). The meshing is done using a free triangular mesh swept on the other parts; the selected size is finer for the study. A time-dependent study validates the temperature time plot with the maximum temperature change in Ossmer *et al.* [40]. The simulation results obtained in Figure 3.5 concluded that the maximum temperature change obtained for the austenite phase is 17 K, which is obtained for the values of constants as C_1 = 0.8 kJ/(kgKGPa) and C_2 = -0.1 kJ/(kgKGPa) as shown in Figure 3.5. It can be observed that while loading the material, the temperature increases, and while unloading, the material temperature decreases. The martensite curve also utilized the same approach, similar to the validation procedure considered in the austenite temperature change validation. The material properties are changed for the martensite phase, which are mentioned in Table 2.1. Figure 3.6 shows the simulation for various values of C_1 and C_2. The temperature change is a function of entropy, which has been

modeled mathematically as a stress function. At the same time, the procedure remains the same for the austenite and martensite phase temperature-time curves.

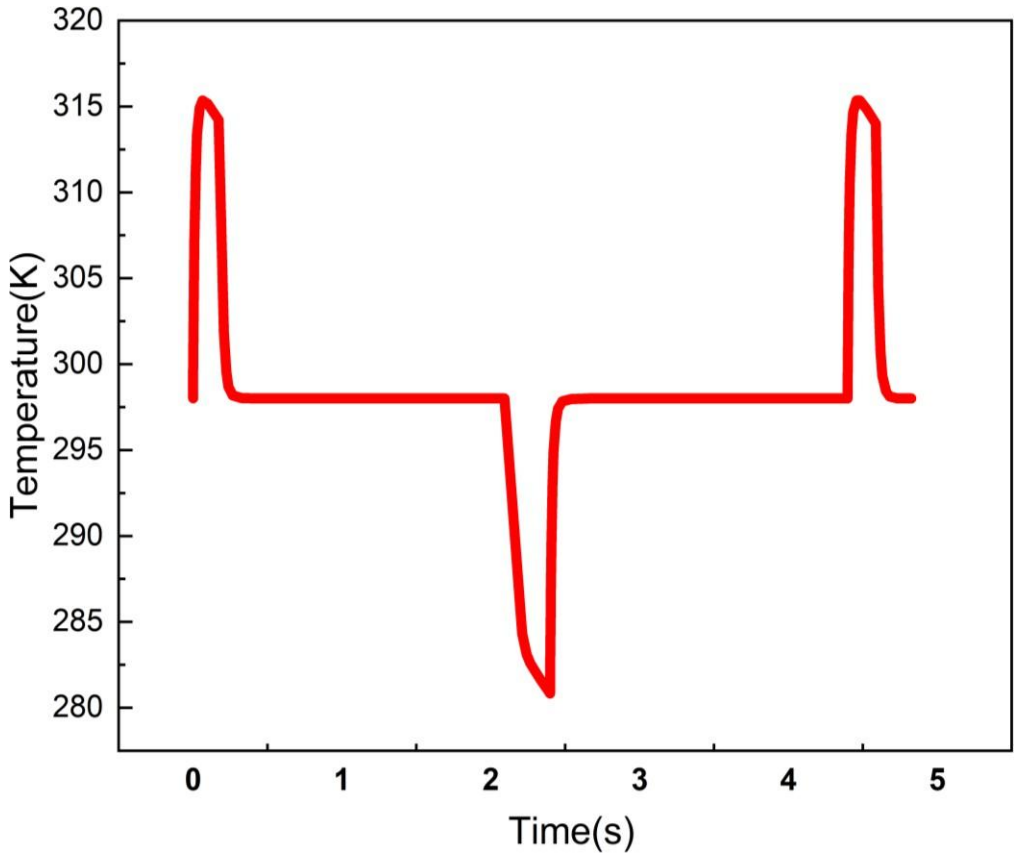

Figure 3.5 Temperature-time validation for the austenite phase.

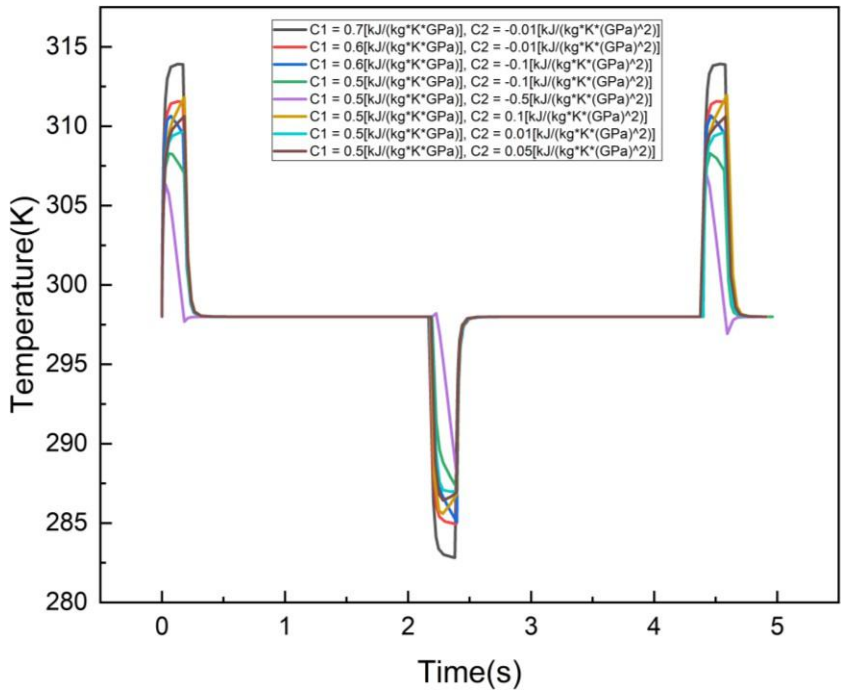

Figure 3.6 Temperature time-varying values of C_1 and C_2 in the stress equation for the martensite phase.

Hence, as shown in Figure 3.5, the temperature change of the martensite phase is obtained as 16 K, which has been validated by the results of Ossmer *et al.* [40]; see Figure 3.7. The values of constants taken in the simulation are C_1 = 0.7 kJ/(kgKGPa) and C_2 = -0.01 kJ/(kgKGPa).

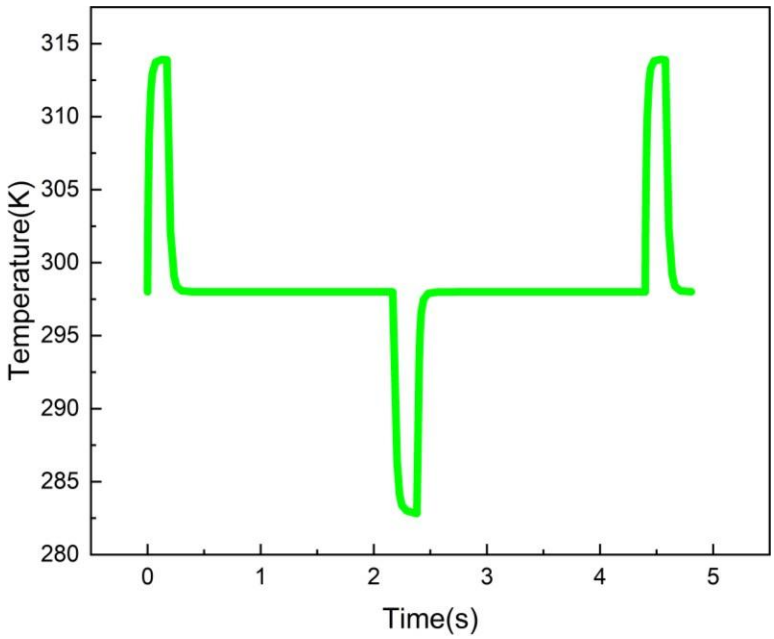

Figure 3.7 Temperature-time validation for the austenite phase.

It is important to note that all the mentioned plots of temperature time are specified using the domain probe function in the definition section of the model builder. The required expression can be searched or written as suitable for the COMSOL simulation. However, the temperature change is obtained separately as the phase change is not obtained in the validation process.

3.4 Temperature time curve validation

The next step is to validate the temperature curve, which suggests that the phase transformation is obtained. In this process, the obtained curve is compared with the results obtained in previous studies. For validating the curve, as shown in Figure 3.8, a 2D geometry is considered with a rectangle having a width of 0.48 mm and a height of 17 mm. An interpolation function is applied with loading and unloading in 0.5 seconds, and the total cycle time is exercised as 60 seconds, which is made periodic using an analytic function. The material parameters are defined in the material section. The solid mechanics module is applied with boundary conditions that apply the analytic function as z-direction prescribed displacement u_{0z} = -17×0.035×an1(t). The shape memory alloy material model is considered in solid mechanics using a Lagoudas model. A roller is selected on the other end of the prescribed displacement end. The heat transfer in solids is defined as a heat source having a general source and total power dissipation density(solid). Also, it utilizes heat flux on one of the surfaces through which heat transfer occurs, with the specified values of heat transfer coefficients of 120

W/m^2K and ambient temperature value; the flux type selected is convective heat flux. Meshing was done using a fine-sized mapped mesh. A time-dependent study is done for three cycles, a three-minute temperature-time cycle plot, as seen in Figure 3.8.

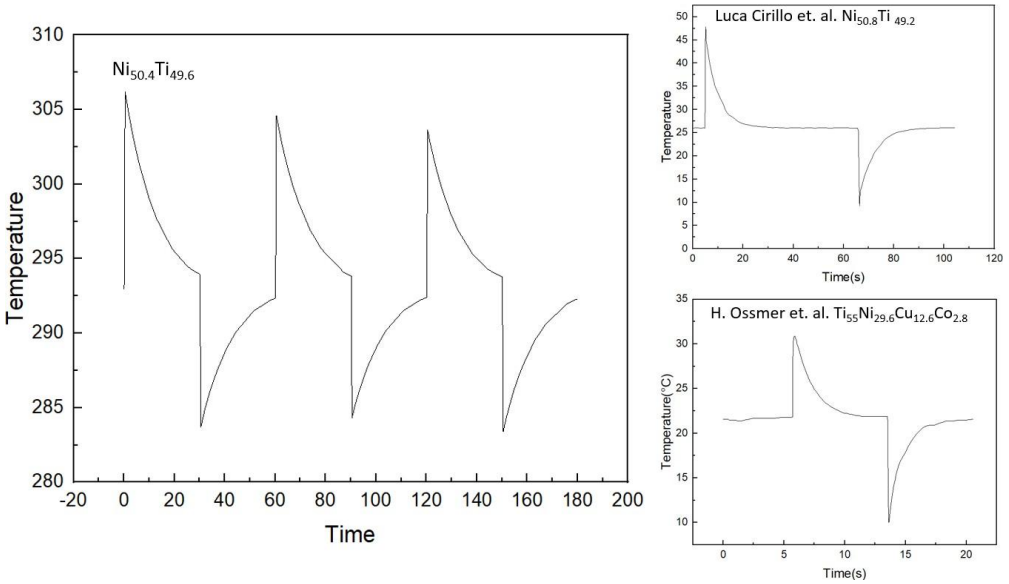

Figure 3.8. Temperature time curve validation [40, 51, 52].

The study is done with the domain probe in the definition section of the model builder in COMSOL. The results obtained in Figure 3.8 for the left side curve [40] are comparable to results available in the literature [51, 52]. The plots have been redrawn for comparison. Hence, the temperature time plot has been validated using simulation results. With the validation results mentioned in this chapter, the final step is to proceed with the results section to apply the eC effect and integrate it with the available approaches for cooling.

3.5 Conclusion

This chapter is a detailed discussion about validating the results from previously available results in the literature. The validation results and procedure to obtain these results have been discussed in detail. The results are utilized to integrate with the available approach for cooling, and it is checked in Chapter 4 whether it can alone be an effective method to be employed.

Chapter 4

Results and Discussion

An eC cooling device needs to cyclically apply uniaxial stress on a material that triggers the eCE. A mechanism needs to be considered to dissipate heat generated in the material. In contrast, during the cooling cycle, the material can absorb the heat from the source to provide a cooling effect. It is observed in all present cooling devices that the heat generated is released into the environment, and the heat flow from the device to be cooled is absorbed into the refrigerant material. This study shows the possibility of integrating an eC cooling device with an existing cooling mechanism. The proposed study suggests that the eC device can provide new insight into the cooling of LEDs applied in automotive headlights or can be considered to cool critical electronic components.

4.1 Introduction

The traditional approach of using compression refrigeration technology poses challenges in meeting the current cooling demands in compact spaces like electronics, for which the proposed eC can prove detrimental. The motivation to tackle the LED in automotive headlights suggests improved life of the LEDs, less power consumption due to reduced temperature, and heat rejection improves the LED's overall performance by increasing the LED's efficiency.

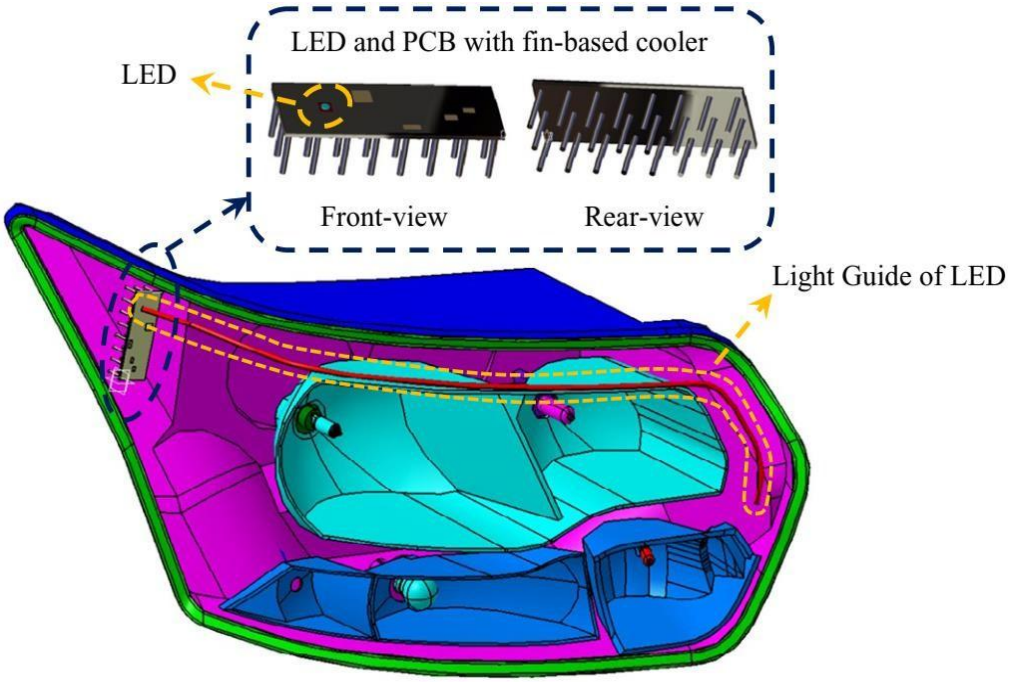

Figure 4.1. 3D model of a real-world automotive lighting system with LED light guide [53].

In recent years, LEDs have been operated extensively in vehicle lighting applications due to their enhanced service life of nearly 100,000 hours, depending on the application. A temperature below 110 ℃ is preferred as it helps dissipate energy more efficiently than the halogen bulbs at 3000 ℃ and 700 ℃ for the

xenon bulbs [53]. This study focused on cooling the LED light guide, as shown in Figure 4.1. The power to be dissipated is 1 W, and a heat sink is taken, as depicted in Figure 4.2. The approach places a NiTi material between the sink and chip, which acts as a heat source. The temperature cycle is applied to the SMA for the results.

4.2 Chip cooling with traditional methods

A chip has been considered, which is assumed to be the source of heat generation or a temperature source. A traditional approach is applied to study the behavior of the source when the sink of aluminum material and airflow are utilized to cool or maintain the source's temperature. A stepwise approach is considered to understand the problem better so a new approach can be integrated while dealing with the problem. The traditional cooling methods include air cooling with natural and forced convection using a fan, a heat sink, a combination of heat sink and air cooling, heat pipes and fan-based air convection cooling. Also, there can be other approaches for cooling, as discussed in Chapter 1.2.1.

Step 1: A Chip increase in temperature without any effective cooling method. For a 1 W chip, the temperature increases to approximately 320 K for a 20-second simulation time.

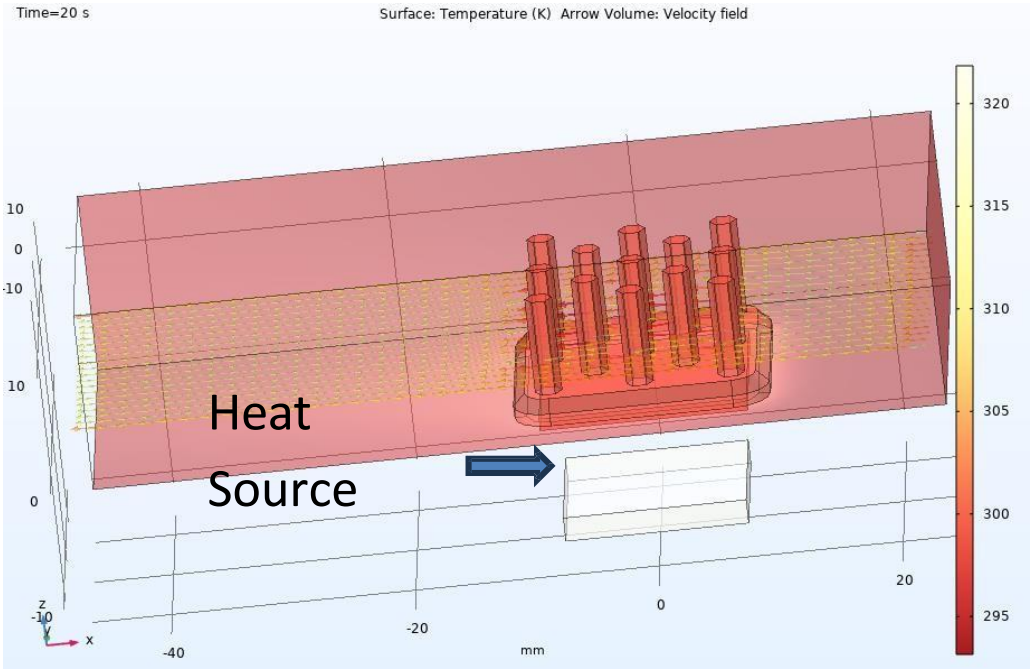

Figure 4.2 Chip temperature without cooling.

Figure 4.2 shows that the heat source can heat at 1 W for 20 seconds. The source temperature is increased, which comes to 320 K from the initial temperature of 293.15 K. The source is heated as no cooling mechanism is available, and it is separated from the sink and the air domain, as clearly visible in Figure 4.1. The dimensions of the heat source are 15 mm ×15 mm × 2 mm. The source is silica glass, an inbuilt material from the COMSOL available model. Hence, only a temperature increase of approximately 27 K in 20 seconds is observed. This

shows that if a significant cooling method is not applied, the chip is expected to further increase in temperature, which is suitable for the chip and the system in which it is integrated. The temperature increase in an LED increases power consumption.

Step 2: When placed with a heat sink, the chip temperature increases. For a 1 W chip, the temperature increases to 301 K approximately in 20 seconds of simulation time.

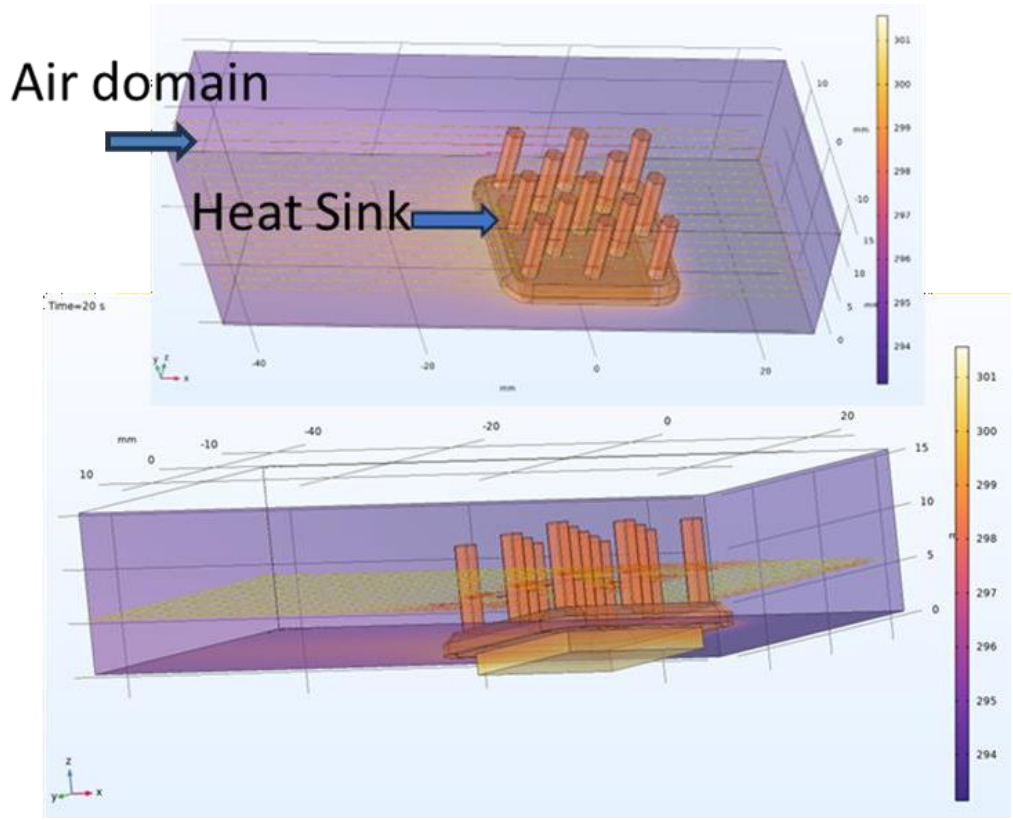

Figure 4.3 Chip temperatures with cooling using a heat sink.

After the results obtained in Figure 4.2, the chip is used for cooling with a heat sink and air domain, as shown in Figure 4.3. The sink is made of aluminum and is utilized from an inbuilt material library in COMSOL Multiphysics. An air domain is also applied to remove heat from the heat sink. The input and output for the air to flow have been specified in the air domain. The air domain is also specified with the material as air, which is an inbuilt material in the material library. It is observed that with the heat sink and air domain with flow at a velocity of 0.05 m/s, the overall temperature is raised to 301 K, which is approximately 8 K for 20 seconds of simulation time. However, it is expected that for a longer duration, the temperature will further increase, which, after some period, may degrade the performance of the chip due to inefficient heat dissipation. This problem can be eliminated by increasing the airflow velocity.

Step 3: Increase the chip temperature for stationary results. For a 1W chip, the temperature increases to approximately 370 K.

The results obtained in Figure 4.4 are further analyzed using a stationary study in COMSOL Multiphysics. The stationary results show that a stable temperature above 370 K is reached when the flow becomes stable. The similar features mentioned in Step 2 are done with only the variation of the study. The airflow is kept at 0.05 m/s. Although it is one of the methods for adequate cooling, newer technologies still need to be integrated to study whether the new technologies perform better or for the slightest improvement; it may prove detrimental.

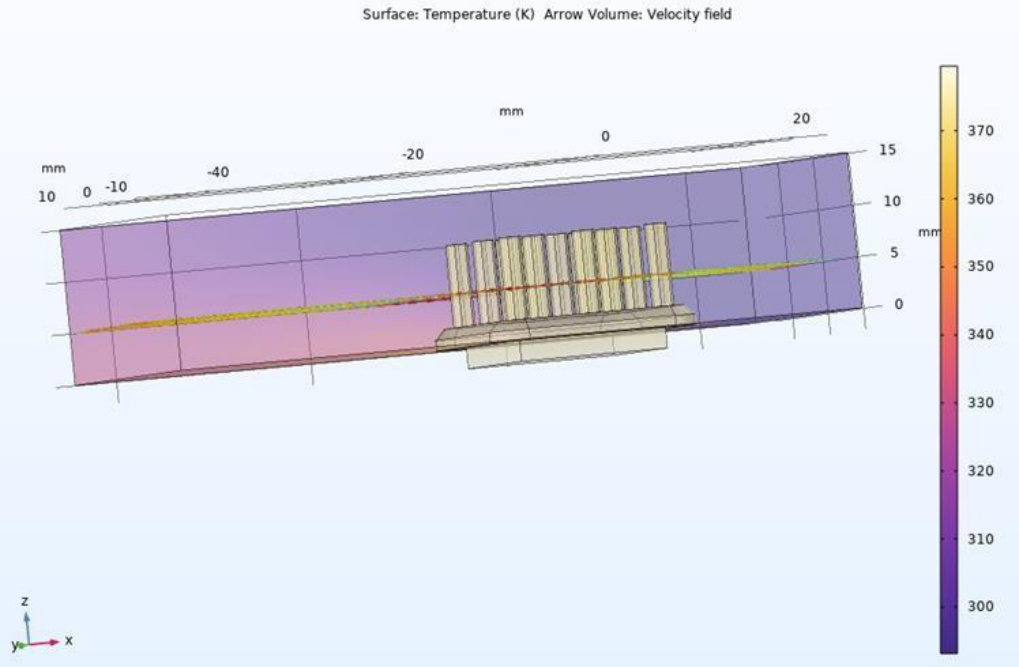

Figure 4.4 Stationary study results for chip cooling.

As visible from Figure 4.4, the stationary results suggest that the overall temperature increase is ~77 K, which gives a temperature of 103 ℃. Thus, the approach integrates eC cooling technique for studying the results with or without temperature cycles, as obtained in Chapter 3.

Step 4: Chip temperature increases with the NiTi plate between the sink and the chip. For a 1 W chip, the temperature increases to approximately 300 K.

In this step, the SMA material was integrated using NiTi between the sink and the source, as shown in Figure 4.5. The results are obtained using a time-dependent study for 20 seconds. It is seen that the temperature increases by nearly 7 K. This is due to conduction heat transfer with the NiTi material having higher thermal conductivity. The NiTi material properties are taken as input from Table 2.1, which is specified in COMSOL Multiphysics using a blank material in the material section. A time-dependent study is done without using the eC effect, analyzing its effect if the material is placed between the heat source and sink. The effect is the simple temperature reduction of approximately 1 K for some time. Hence, if the SMA material is applied, it may decrease the source's temperature by some percentage, which has been discussed further in Figure 4.7. These above

steps form the basis for further analysis. The dimensions of the NiTi plate are made to be 17mm x 17mm x 1 mm.

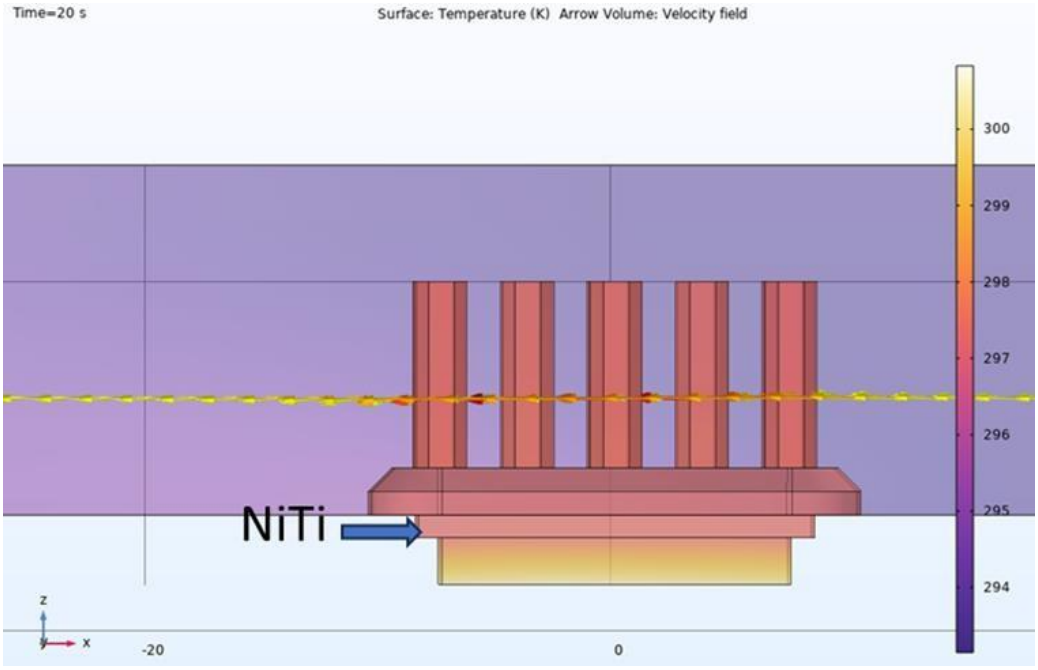

Figure 4.5 Chip temperature with NiTi plate without temperature cycles.

All the steps mentioned above employ the heat transfer in solids and fluids module and a laminar flow module, which have been coupled using the non-isothermal flow in COMSOL Multiphysics. The heat source material generates heat of 1 W, and all geometries are allotted the initial temperature of 293.15 K. Further, the above-mentioned steps are plotted for a longer time to analyze the effect under different conditions. Figure 4.6 is a continuation of step 2, in which the time limit of the study is increased from 20 seconds to approximately 3 minutes. The results clearly show an increase in the temperature of both a heat source and a heat sink. The temperature of the heat source reaches nearly 355 K. Here, the heat source is specified as an initial temperature of 313.15 K, and the heat source is specified as 1 W. The air domain is considered to have no flow.

In continuation of step 4, Figure 4.7 shows the source and sink temperature variation when the SMA material NiTi is only placed between the sink and source. Figure 4.7 (a) shows a temperature increase without the flow of air, which is reduced compared to that without applying NiTi, as depicted in Figure 4.6. The temperature rise in Figure 4.7 (a) is approximately 340 K. In Figure 4.7 (b), a flow velocity is 0.25 m/s, significantly reducing the temperature rise of both sink and source to 318 K and 316 K, respectively. The initial source temperature has been specified to be 313.15 K with a heat source of 1 W. The simulation has been done for 3 minutes. This study shows how an SMA without an eC effect can be helpful compared to traditional methods.

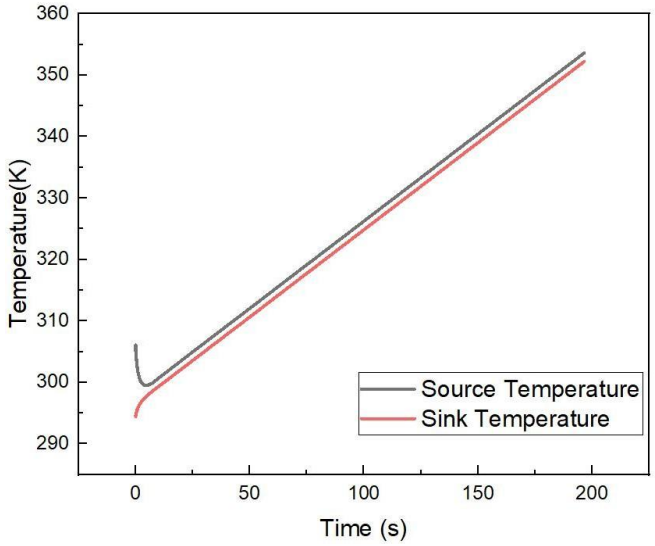

Figure 4.6 Chip and heat sink temperature over time with heat generation (Q = 1W)

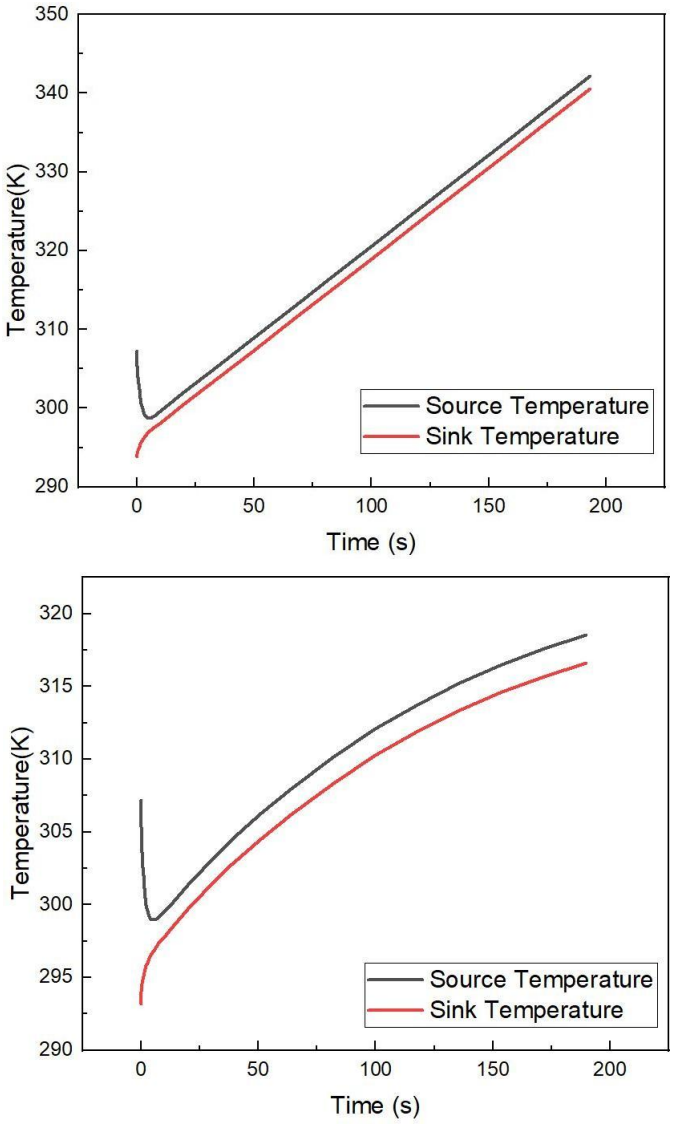

Figure 4.7 Chip temperature and heat sink temperature with NiTi plate without temperature cycles (a) without airflow (v = 0), (b) with airflow (v = 0.25 m/s).

4.3 ECE integration with traditional methods for cooling

Figure 4.8 considers the application of eC cooling cycles on the SMA material. The results obtained are depicted in Figure 4.8. The results are obtained by taking the heat transfer temperature function in the solids and fluids module. The temperature is only specified on all the surfaces of the NiTi material. The input temperature function is an interpolation function containing the input as cooling cycles from the validation curves obtained in the previous chapter. The heating cycles are not considered, as the mechanism to be considered is that the SMA material will be in contact with the heat source only during the constant load after unloading the material. The initial temperature of the heat source is 313.15 K, and the heat source has a heat generation of 1 W.

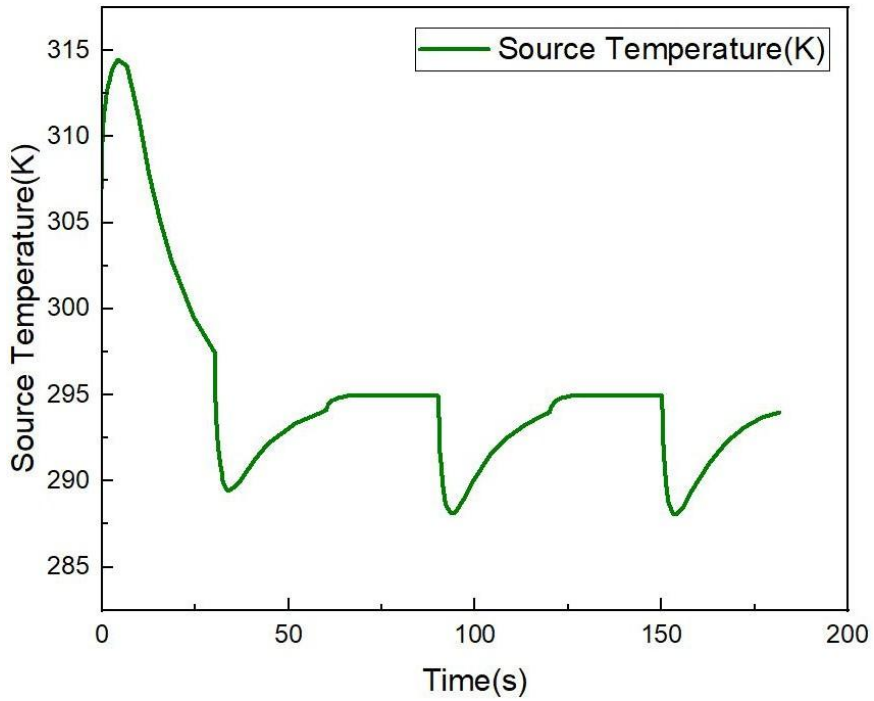

Figure 4.8 Chip temperatures with NiTi plate with temperature cycles.

As observed from Figure 4.8, initially, as the cycle starts, the temperature of the heat source increases from 307.05 K to 314.51 K due to heat generation in the source material. However, the temperature drops significantly after this, which follows the cooling cycle. Thus, as there is sufficient time after unloading the material, the temperature increases after the material is unloaded. This cycle of unloading and holding is continuous, and the heat source can reject its temperature continuously to the SMA material; hence, the curve shown in Figure 4.8 is maintained at ambient temperature and below ambient during unloading. Based on the simulation results, the proposed eC effect has proven suitable. The study is focused on cooling the heat source, which has dimensions of 1.5 cm × 1.5 cm × 2 mm, by integrating an eC material with the eC cooling.

Chapter 5

Conclusions and Future Outlook

5.1 Conclusion

The SMA material in this study has high eC temperature change and is scalable and environmentally friendly. COMSOL Multiphysics simulates the eCE, considering NiTi as eC material. Equation-based modeling is done for eC temperature change estimation. The stress field is utilized in the trapezoidal form as an input to the material with very short input and large holding time to obtain maximum eCE. The temperature cycles are obtained using the stress input in 0.5 seconds while holding the material at this stress for 29.5 seconds, similar to unloading and holding times. The operating temperature is varied for validation purposes. A temperature of 313.15 K is applied for the source material, while the sink is set to 293.15 K as the initial temperature. Thermal contact loss was neglected in this study, using thermal grease between the contact surfaces. The temperature cycles thus obtained are applied using a NiTi material between the heat sink and the source of heat generation. The geometry considered for cooling is a rectangular plate having dimensions of 15 mm × 15 mm and a thickness of 2 mm. A single temperature cycle of 60 seconds is obtained using stress cycles of the same period. Loading and unloading lead to major increases and decreases in temperature, which occur in a short period of 0.5 seconds. The mechanism considered in this study is based on conduction heat transfer due to the touch between the SMA material and the heat source during unloading and holding so that it gains heat from the heat source material. Similarly, during the loading and holding period, after loading, the SMA is considered to be in contact with the sink to reject the heat.

However, in this study, a small chip is considered to be cooled, and a plate geometry is examined, considering the cooling of the light guide of the LED, which consumes a comparatively smaller amount of power. However, it is necessary to consider a wire-like geometry with enhanced heat transfer characteristics to cool a high-power source. The proposed study of an eC device can overcome issues of chip overheating for electronics applications or an LED headlamp cooling, increasing the overall efficiency of the device and leading to low power generation while producing the maximum amount of luminance without an increase in consumption power input. This study is also a basis for studying eC characteristics for cooling other critical electronics, refrigeration, and air conditioning applications.

5.2 Limitation/assumption behind the proposed simulation work

- The assumption is that the EC device only comes into contact with the heat source when it is overheated, and the EC device is withdrawn when it reaches room temperature. Whenever the chip overheats, the EC device

comes into contact with it. So, taking these factors into account, the current study was conducted.

- All sides except the top layer are assumed to be insulated, and heat is released from the top layer.
- The heat transfer is assumed only through conduction from the heat source to the NiTi material.
- To simplify the simulation, it is considered that there is no loss due to thermal contact using thermal grease between the layers of contact.

5.3 Future Outlook

Boosting the isothermal heat transfer and the adiabatic temperature change across a wide temperature range while using relatively low mechanical stress remains a key challenge for developing practical eC solid-state cooling systems. Additionally, eC materials must be engineered for better mechanical durability, thermal stability, and resistance to functional fatigue to ensure they can withstand repeated application in real-world devices. Key focus areas for eC device development are

i. Thermal switching efficiency: Optimize designs to ensure rapid, reliable heat transfer between the eC material (e.g., NiTi wires/sheets) and heat sinks/sources during cyclic mechanical loading/unloading.

ii. Material-to-device integration: Translate lab-scale eC materials (fatigue-resistant NiTi alloys) into compact, scalable prototypes. Prioritize cyclic stability under repeated stress ($>10^4$ cycles) and compatibility with actuators.

iii. Cascade systems for broad temperature ranges: Design multi-stage eC cooling systems using materials with staggered transformation temperatures (NiTi, Cu-Al-Mn alloys) to widen operational ranges. Address challenges like parasitic heat loss and synchronization of phase transitions across stages.

iv. Loss mitigation strategies: Quantify and minimize: Hysteresis losses (energy dissipation during stress cycles), parasitic heat leaks from imperfect insulation.

v. Ideal eC material properties: High adiabatic $\Delta T/\Delta S$: Achieve >10 K temperature change under low stress (<200 MPa). Durability: Resist functional fatigue (grain refinement in NiTi to suppress dislocation). Temperature-stable performance: Consistent eCE across operating conditions (250–350 K). Low interfacial resistance: Ensure seamless thermal contact between eC material and heat exchangers.

By addressing these areas, eC cooling can transition from lab innovation to real-world sustainability solutions.

References:

1. Peters, T. and L. Sayin, *Future-proofing sustainable cooling demand*. 2022, ADBI Working Paper.
2. programme, U.e. *The Montreal Protocol*. UN Environment Programme 1987; Available from: https://www.unenvironment.org/ozonaction/who-we-are/about-montreal-protocol.
3. Ho-Ming Tong, Y.-S.L., C.P. Wong, *Advanced Flip Chip Packaging*. 2013: Springer.
4. STANDARDS, B.O.I., *IS 17550: Part 1: 2021: HOUSEHOLD REFRIGERATING APPLIANCES CHARACTERISTICS AND TEST METHODS* in *Part 1 General Requirements, Bureau of Indian Standards*. 2021.
5. Brüderlin, F., *Advanced elastocaloric cooling devices based on shape memory alloy films*. 2022: KIT Scientific Publishing.
6. Mahan, G. *Multilayer thermionic refrigeration*. in *Eighteenth International Conference on Thermoelectrics. Proceedings, ICT'99 (Cat. No. 99TH8407)*. 1999. IEEE.
7. Brown, D.R., et al., *The prospects of alternatives to vapor compression technology for space cooling and food refrigeration applications.* Energy Engineering, 2012. **109**(6): p. 7-20.
8. De Waele, A., *Pulse-tube refrigerators: principle, recent developments, and prospects.* Physica B: Condensed Matter, 2000. **280**(1-4): p. 479-482.
9. Besagni, G., R. Mereu, and F. Inzoli, *Ejector refrigeration: A comprehensive review.* Renewable and Sustainable Energy Reviews, 2016. **53**: p. 373-407.
10. WIKIPEDIA. *Vortex tube*. 2024 [cited 2025; Available from: https://en.wikipedia.org/wiki/Vortex_tube.
11. Blank, D. and C. Wu, *Cooling and heating rate limits of a reversed reciprocating Ericsson cycle at steady state.* Proceedings of the Institution of Mechanical Engineers, Part A: Journal of Power and Energy, 2000. **214**(1): p. 75-85.
12. Deserranno, D. *Reverse-Brayton Cryocoolers*. 2025; Available from: https://www.conceptsnrec.com/blog/reverse-brayton-cryocoolers-.
13. Vijayaraj, T., et al., *Application of the thermoacoustic effect to cooling of air using acoustic waves.* Int J Adv Res Innovative Ideas Educ, 2017. **3**(5): p. 67-72.
14. Brown, J.S. and P.A. Domanski, *Review of alternative cooling technologies.* Applied Thermal Engineering, 2014. **64**(1-2): p. 252-262.
15. *Desiccant Cooling System*. Available from: https://nzeb.in/knowledge-centre/hvac-2/desiccant-cooling-system/.
16. *Heat of Reaction*. Available from: https://www.mt.com/in/en/home/applications/L1_AutoChem_Applications/Process-Safety/heat-of-reaction.html.

17. Rice, W. and G.C. Beakley, *Characteristics of the hydraulic refrigeration system (HRS) using n-butane as the refrigerant.* Energy conversion and management, 1992. **33**(10): p. 943-950.
18. *Absorption Refrigeration System.* SCIENCEDIRECT, 2017.
19. NagaMalleswara Rao, K., M. Ram Gopal, and S. Bhattacharyya, *Analysis of a SrCl2–NH3 solid sorption refrigeration system.* International Journal of Low-Carbon Technologies, 2015. **10**(4): p. 365-373.
20. Nawaz, K. and K. Gluesenkamp, *Separate sensible and latent cooling systems: A critical review of the state-of-the-art and future prospects.* 2018.
21. *Latent heat in cooling towers*. 2023; Available from: https://www.torraval.com/en/latent-heat-in-cooling-towers/.
22. Moya, X., S. Kar-Narayan, and N.D. Mathur, *Caloric materials near ferroic phase transitions.* Nature materials, 2014. **13**(5): p. 439-450.
23. Fähler, S., et al., *Caloric effects in ferroic materials: new concepts for cooling.* Advanced Engineering Materials, 2012. **14**(1-2): p. 10-19.
24. Zhang, J., et al., *Electrocaloric effect in ferroelectric materials: From phase field to first-principles based effective Hamiltonian modeling.* Materials Reports: Energy, 2021. **1**(3): p. 100050.
25. Ožbolt, M., et al., *Electrocaloric refrigeration: thermodynamics, state of the art and future perspectives.* International journal of refrigeration, 2014. **40**: p. 174-188.
26. Patel, S., *Investigation of solid state refrigeration potential in ba0. 85ca0. 15zr0. 1ti0. 9o3-based ferroelectric ceramics (PHD)*. 2016, IITMandi.
27. Barman, A., S. Kar-Narayan, and D. Mukherjee, *Caloric effects in perovskite oxides.* Advanced Materials Interfaces, 2019. **6**(15): p. 1900291.
28. Li, X., et al., *Pyroelectric and electrocaloric materials.* Journal of Materials Chemistry C, 2013. **1**(1): p. 23-37.
29. Strässle, T., et al., *A novel principle for cooling by adiabatic pressure application in rare-earth compounds.* Journal of Alloys and Compounds, 2000. **303**: p. 228-231.
30. Xie, Z., G. Sebald, and D. Guyomar, *Comparison of elastocaloric effect of natural rubber with other caloric effects on different-scale cooling application cases.* Applied Thermal Engineering, 2017. **111**: p. 914-926.
31. Bonnot, E., et al., *Elastocaloric effect associated with the martensitic transition in shape-memory alloys.* Physical review letters, 2008. **100**(12): p. 125901.
32. Qian, S., et al., *High-performance multimode elastocaloric cooling system.* Science, 2023. **380**(6646): p. 722-727.
33. Mevada, H., et al., *Elastocaloric Cooling: A Pathway Towards Future Cooling Technology: Refroidissement élastocalorique: une voie vers une future technologie de refroidissement.* International Journal of Refrigeration, 2024.

34. Zhang, Z., X. Wang, and Y. Yan, *A review of the state-of-the-art in electronic cooling.* e-Prime-Advances in Electrical Engineering, Electronics and Energy, 2021. **1**: p. 100009.
35. Holme, *VII. A description of a property of caoutchouc, or indian rubber; with some reflections on the cause of the elasticity of this substance. In a letter to Dr. Holme.* The Philosophical Magazine, 1806. **24**(93): p. 39-43.
36. Joule, J.P., *V. On some thermo-dynamic properties of solids.* Philosophical Transactions of the Royal Society of London, 1859(149): p. 91-131.
37. Mañosa, L. and A. Planes, *Materials with giant mechanocaloric effects: cooling by strength.* Advanced Materials, 2017. **29**(11): p. 1603607.
38. Qian, S., et al., *Thermodynamics cycle analysis and numerical modeling of thermoelastic cooling systems.* International Journal of Refrigeration, 2015. **56**: p. 65-80.
39. Ossmer, H., et al. *Elastocaloric cooling using shape memory alloy films*. in *Journal of Physics: Conference Series*. 2013. IOP Publishing.
40. Ossmer, H., et al., *Evolution of temperature profiles in TiNi films for elastocaloric cooling.* Acta materialia, 2014. **81**: p. 9-20.
41. Tušek, J., et al., *Elastocaloric effect of Ni-Ti wire for application in a cooling device.* Journal of Applied Physics, 2015. **117**(12).
42. Sokolovskiy, V., et al., *Monte Carlo Simulations of Thermal Hysteresis in Ni-Mn-Based Heusler Alloys.* physica status solidi (b), 2018. **255**(2): p. 1700265.
43. Liu, B., Y. Wang, and W. Wu, *Effects of Thermal Cycling and Porosity on Phase Transformation of Porous Nanocrystalline NiTi Shape Memory Alloy: An Atomistic Simulation.* Advanced Engineering Materials, 2023. **25**(21): p. 2301019.
44. Bachmann, N., et al., *Modeling of an elastocaloric cooling system for determining efficiency.* Energies, 2022. **15**(14): p. 5089.
45. Bachmann, N., et al., *Phenomenological model for first-order elastocaloric materials.* International Journal of Refrigeration, 2022. **136**: p. 245-253.
46. Chen, Y., et al., *A compact elastocaloric refrigerator.* The Innovation, 2022. **3**(2).
47. Li, X., S. Cheng, and Q. Sun, *A compact NiTi elastocaloric air cooler with low force bending actuation.* Applied Thermal Engineering, 2022. **215**: p. 118942.
48. Cirillo, L., et al., *Numerical optimization of a single bunch of niti wires to be placed in an elastocaloric experimental device: preliminary results.* Magnetochemistry, 2021. **7**(5): p. 67.
49. Cirillo, L., A. Greco, and C. Masselli, *Development of an electronic circuit cooling system using elastocaloric effect: a FEM comparison among different configurations.* Applied Thermal Engineering, 2023. **219**: p. 119463.
50. Provon. *LED Headlights*. 2025; Available from: https://privon.in/products.
51. Ossmer, H., et al., *Local evolution of the elastocaloric effect in TiNi-based films.* Shape Memory and Superelasticity, 2015. **1**: p. 142-152.

52. Cirillo, L., A. Greco, and C. Masselli, *A numerical comparison among different solutions for the design of a rotary elastocaloric prototype.* Applied Thermal Engineering, 2023. **228**: p. 120487.
53. Sökmen, K.F., E. Yürüklü, and N. Yamankaradeniz, *Computational thermal analysis of cylindrical fin design parameters and a new methodology for defining fin structure in LED automobile headlamp cooling applications.* Applied Thermal Engineering, 2016. **94**: p. 534-542.